Journal of
Marine Science and Engineering

MDPI

Review

Role of Upper-Flow-Regime Bedforms Emplaced by Sediment Gravity Flows in the Evolution of Deltas

Svetlana Kostic [1,*], Daniele Casalbore [2], Francesco Chiocci [2], Jörg Lang [3] and Jutta Winsemann [3]

[1] Computation Science Research Center, San Diego State University, San Diego, CA 92182, USA
[2] Sapienza University of Rome, 00185 Rome, Italy; daniele.casalbore@uniroma1.it (D.C.); francesco.chiocci@uniroma1.it (F.C.)
[3] Institute for Geology, Leibniz University Hannover, 30167 Hannover, Germany; lang@geowi.uni-hannover.de (J.L.); winsemann@geowi.uni-hannover.de (J.W.)
* Correspondence: skostic@sdsu.edu

Received: 20 November 2018; Accepted: 27 December 2018; Published: 4 January 2019

Abstract: Upper-flow-regime bedforms and their role in the evolution of marine and lacustrine deltas are not well understood. Wave-like undulations on delta foresets are by far the most commonly reported bedforms on deltas and it will take time before many of these features get identified as upper-flow-regime bedforms. This study aims at: (1) Providing a summary of our knowledge to date on deltaic bedforms emplaced by sediment gravity flows; (2) illustrating that these features are most likely transitional upper-flow-regime bedforms; and (3) using field case studies of two markedly different deltas in order to examine their role in the evolution of deltas. The study combines numerical analysis with digital elevation models, outcrop, borehole, and high-resolution seismic data. The Mazzarrà river delta in the Gulf of Patti, Italy, is selected to show that upper-flow-regime bedforms in gullies can be linked to the onset, growth, and evolution of marine deltas via processes of gully initiation, filling, and maintenance. Ice-marginal lacustrine deltas in Germany are selected as they illustrate the importance of unconfined upper-flow-regime bedforms in the onset and evolution of distinct delta morphologies under different lake-level trends.

Keywords: marine and lacustrine deltas; transitional upper-flow-regime bedforms; cyclic steps; antidunes; delta evolution; confined or unconfined setting; foreset-bottomset transition; gullies

1. Introduction

Deltas can be classified based on a variety of criteria. The most conventional, process-based classification defines delta types depending on the relative contribution of fluvial, wave, or tidal energy flux that was dominant during deposition at the seaward edge of the delta [1–3]. Other classifications of deltas emphasize foreset/topset geometry [4,5], sediment grain size [2], or delivery system type [6–8]. More recent studies demonstrate that external geometry and internal characteristics of deltas greatly vary in response to the falling and rising of sea level [9–13]. This paper focuses on upper-flow-regime bedforms observed on diverse deltas in marine and lacustrine settings at water depths of up to about 150–200 m. Parts of deltas that extend beyond water depths of 200 m are not investigated herein.

Upper-flow-regime bedforms on deltas may have a crucial role in their onset, growth, and evolution. Yet, they are far less documented and understood than their deep-sea counterparts. Upper-flow-regime bedforms on deep-sea fans have received a growing recognition in the last decade or so. They have been documented numerically (e.g., References [14–16]), experimentally (e.g., Reference [17]), and in the field (e.g., References [18–23]).

When it comes to deltas, the most commonly reported bedforms are undulated sediment features on delta foresets (e.g., References [24–26]). The term that is frequently used to describe them is sediment

waves or sediment undulations. Sediment waves on the Mediterranean deltas, which are among the most extensively studied deltas, have been reported for the last thirty years [26–43]. Early on, they were interpreted as sediment deformation and slope failure features [27–30,32–35]. More recently, these interpretations were seriously questioned and it was proposed that many fields of sediment waves were in fact formed by sediment transport processes [26,38,39]. Mixed theories suggesting, i.e., initial sediment deformation and growth by differential sediment accumulation patterns were also proposed (e.g., Reference [37]).

The interpretation of deltaic sediment waves has potentially significant implications for offshore and coastal management, especially along heavily populated coastlines worldwide (e.g., References [26,44]). The scientific community is still debating on a genetic mechanism to these features and it will take time before many of them get identified as upper-flow-regime bedforms emplaced by sediment gravity flows (e.g., References [15,16]).

Recent research on the Squamish delta [45–47], Mazzarrà delta [48], and (glacio) lacustrine deltas (i.e., References [49–51]) has significantly improved our understanding of upper-flow-regime bedforms on deltas. The aim of this paper is to: (a) Provide a summary of our knowledge to date; (b) demonstrate that these features in both confined and unconfined environments are most likely transitional upper-flow-regime bedforms; and (c) use field case studies of the Mazzarrà delta in Italy and glaciolacustrine deltas in Northern Germany in order to examine their role in the evolution of deltas.

Terminology used to describe deltaic deposits in the literature can be very confusing. Thus, an effort was made herein to adopt terminology that is clear and generally applicable (Figure 1). For fine-grained deltas, the term delta plain is used concurrently with the term topset deposit, whereas the prodelta slope incorporates foreset and bottomset deposits. For coarse-grained deltas, the terms delta plain and delta slope are used concurrently with topset and foreset deposit, respectively.

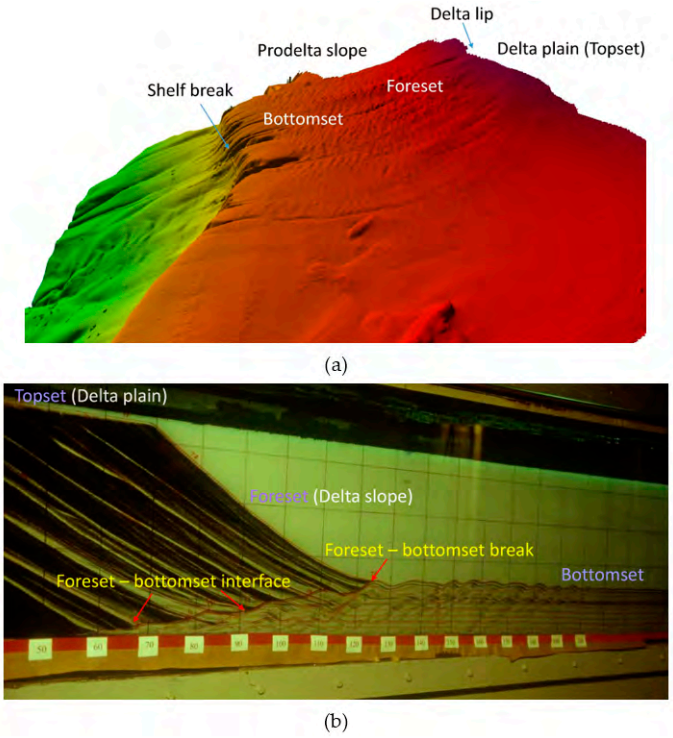

Figure 1. Terminology for fine-grained and coarse-grained deltas: (**a**) 3-D view of the Mazzarrà river delta, Italy. The location of the delta plain/ lip is only tentative as the 3-D coverage does not extend to the delta plain. The flow was from right to left. (**b**) Gilbert-type delta reproduced experimentally at St. Anthony Falls Laboratory, USA (Experiment 2 in Kostic and Parker [43]). The flow was from left to right.

2. Summary of Knowledge to Date

2.1. What Was Learned from Studies on Mediterranean Deltas?

Urgeles et al. [26] offer a very detailed account of the relevant multidisciplinary investigations of the Mediterranean deltas (Figure 2). They combine previously published data with newly acquired high-resolution data to scrutinize the origin of the Mediterranean deltaic sediment waves. The previously published data were found to be of very differing resolution, penetrations, spatial and temporal coverage. They include shallow water multibeam echosounder [37–39,42,52], seismic reflection profiles [28–31,33,34,37–41,52,53], high resolution 3D seismic data [36], hydrodynamic time series and hydrographic transects across undulated seafloor features [54], and sediment samples for geotechnical tests and CPT in-situ measurements [55,56]. The new data of Urgeles et al. [26] is comprised of ultra-high resolution seismic and bathymetric data, as well as the sediment core data. Their work demonstrates that: (i) Sediment waves on several Mediterranean deltas appear incompatible with a genesis by sediment deformation alone and do not show evidence of sediment deformation, and (ii) the variety of features observed in the Mediterranean deltaic sediment wave fields can be explained by sediment transport processes, such as internal waves, hyperpycnal flows, bottom currents, and longshore currents. Most importantly, Urgeles et al. [26] noted the similarity between cyclic steps identified by Fildani et al. [18] on the Monterey fan off central California and upslope migrating sediment undulations on prodelta slopes of some Mediterranean deltas. They introduced, for the first time, the idea that some of them could be cyclic steps due to hyperpycnal flows. Based on the literature, the Po river [57,58], the streams of Mediterranean Andalusia [59,60], and the Llobregat river [61] should have concentrations of suspended sediment high enough to allow for the formation of hyperpycnal flows at the river mouth and subsequent turbidity currents overriding the prodelta slope. Thus, upper-flow-regime bedforms are likely to emerge on the Po delta, and the Verde, Seco, Guadalfeo, Gulachos, Albunol, and Adra delta of Mediterranean Andalusia (Figure 2). The majority of deltas of Mediterranean Andalusia display sediment waves on their prodelta slopes. Only sediment waves of the Verde and Seco deltas occur on the channel flanks and are attributed to overtopping of turbidity currents. In the Po river deltaic wedge, the focus is on the area displaying sediment waves that has been linked to flood deposits due to hyperpycnal flows [62]. Additionally, at least some sediment wave fields on the Llobregat delta should be upper-flow-regime bedforms generated by turbidity currents (Figure 3), even though internal waves have been observed to play a major role in resuspending and transporting sediment in undulated areas of this delta [63].

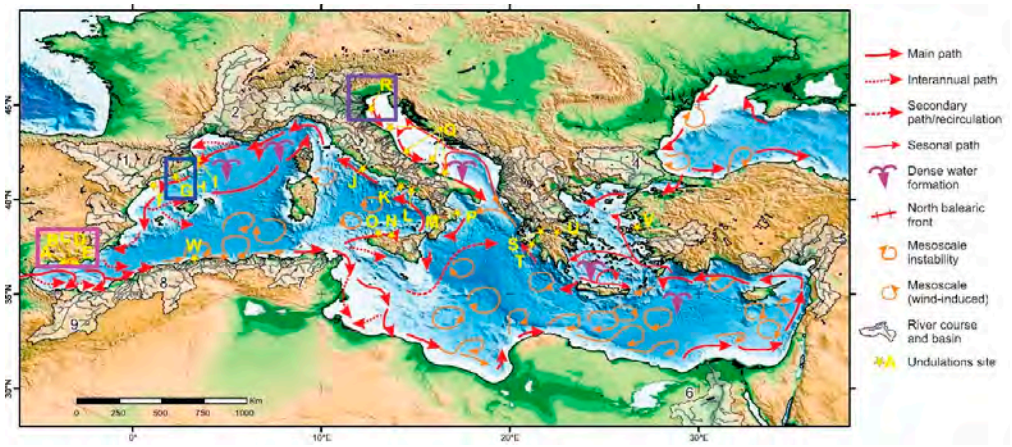

Figure 2. Distribution of sediment waves on deltas of the Mediterranean Sea (yellow stars) in relation to surface oceanographic circulation patterns [26] (Reproduced with permission from Springer, 2011). Upper-flow-regime bedforms formed by turbidity currents due to hyperpycnal flows can be expected on the deltas of Mediterranean Andalusia (blue rectangle), Po river delta (pink rectangle), and the Llobregat river delta (purple rectangle). Image curtesy of Roger Urgeles.

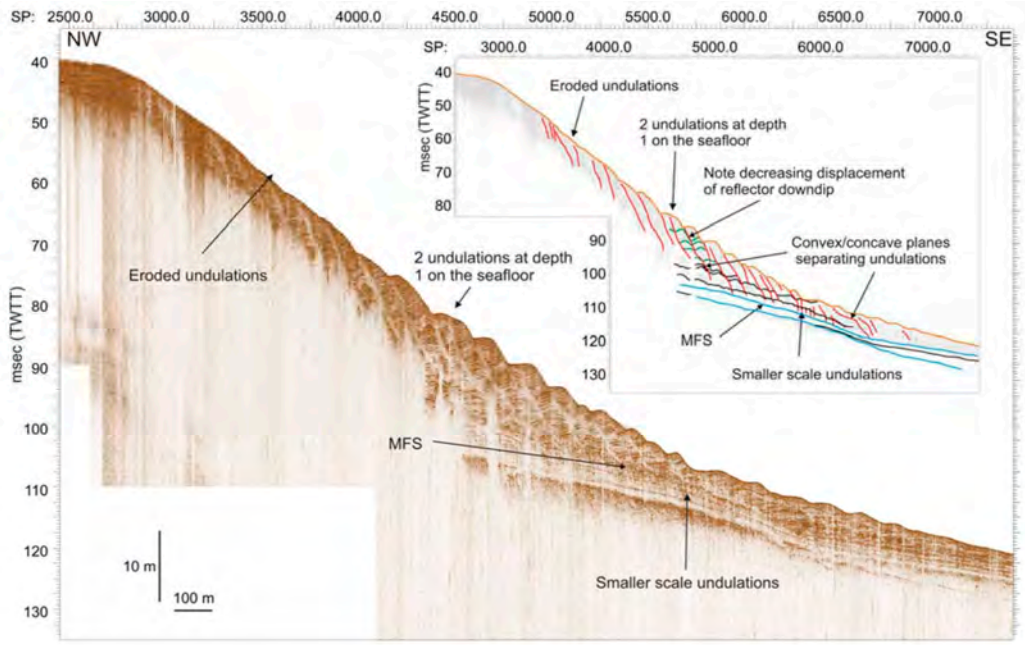

Figure 3. Seismic profile of sediment waves on the Llobregat prodelta slope [26] (Reproduced with permission from Springer, 2011). Waves are rooted at the Maximum Flooding Surface (MFS). The inset explains the interpretation of sediment waves as sediment transport features. Image curtesy of Roger Urgeles.

It is important to note that sediment waves on Mediterranean deltas have wavelengths that are at least an order of magnitude smaller than upper-flow-regime bedforms identified on deep-water fans, i.e., 20–300 m vs. 1–7 km [26]. Their amplitude varies from a few centimeters to up to 5 m. They are found in water depths ranging from 20 to 100 m, on slopes between 0.2° and 3° (an average slope is 2°). The undulations often show an intricate pattern of bifurcating and truncated ridges and can extend down the slope for distances ranging from a few tens of meters to 2 km.

Our analysis of bedforms on deltas of Mediterranean Andalusia in Table 1 uses the methodology of Farrell and Stephan [64] for plunging flows. The total friction coefficient on prodelta slopes is assumed to be of the order of 0.002. The minimal water depth at which bedforms have been observed is assumed to loosely provide some measure of the plunging depth. The estimated turbidity current depth H on prodelta slopes after plunging is used to calculate the ratio L/H of undulation wavelength to flow depth. This ratio suggests that sediment waves on deltas of Mediterranean Andalusia are likely transitional upper-flow-regime bedforms. Exceptions are the Seco and Verde deltas, with their sediment waves more likely being cyclic steps due to a very different setting, i.e., channel flanks rather than prodelta slopes.

Table 1. Analysis of sediment waves on prodeltas of Mediterranean Andalusia.

Delta	Prodelta Slope S [a]	Bedform Wavelenght L (m) [a]			Mixing Coefficient γ [b]	Flow Depth H (m) [b]	Ratio L/H	
		Min	Max	Avg			Min	Max
Verde	0.087	38	103	73	1.27	4.6	8.2	22.3
Seco	0.070	25	74	46	1.13	1.6	15.9	47.0
Guadalfeo	0.044	19	252	80	0.86	5.5	3.4	45.6
Gulachos	0.065	19	140	53	1.08	6.9	2.8	20.4
Albunol	0.079	23	163	61	1.21	4.7	4.9	35.0
Adra	0.054	21	244	76	0.97	9.7	2.2	25.1

Note: [a] data from Urgeles et al. [26], [b] estimated using the methodology of Farrell and Stefan [64].

The growth and maintenance of sediment waves on the Mediterranean deltas by way of hyperpycnal flows is questionable nowadays. Water and sediment discharges have drastically decreased by a host of human activities, including dam construction, river regulation, and urbanization [65–67]. When hyperpycnal flows do form, their frequency and contribution does not seem to be sufficient to counterbalance the competing effect of sea waves [54].

2.2. What Was Learned from Recent Studies on Squamish Delta?

Fjord delta environments have been found to be particularly suitable for monitoring of turbidity currents since shallower depths are easier on instrumentation and turbidity currents occur quite frequently [47,68]. A geophysical monitoring program of the active Squamish delta in the upper Howe Sound, British Columbia (Figure 4) is likely the most detailed monitoring program of a fjord-head delta to date. This program was originally established to investigate the timing and character of submarine mass wasting using integrated multibeam sonar systems [69]. Repeat bathymetric surveys (one–three day period during four months; 70–100 kHz, 1 m horizontal and ~30 cm vertical resolution) of the Squamish delta established occasional, aperiodic delta-lip failures, and frequent/daily upstream migration of crescent-shaped sediment waves within all three channels on the delta slope [46,47]. The location of channels is shown in Figure 4a. Crescent-shaped features were interpreted as cyclic steps because of their upstream migration [47]. During the monitoring period, over hundred mass movements were detected in the channels, with the majority (49) occurring in the Northern channel, which has an average slope of 6°. Small sediment waves (30–70 m wavelength; 2–3 m wave height) dominate its floor, as illustrated in Figure 4b.

Covault at al. [23] applied the morphodynamic model of Kostic [15] to crescent-shaped sediment waves in the Northern channel to demonstrate that these features are likely transitional upper-flow-regime bedforms emplaced by turbidity currents. The numerical results in Figure 4c show a growing train of upstream migrating cyclic steps emerging close to the top of the delta slope and antidunes occupying the downstream end of the channel. The controls on the formation of upper-flow-regime bedforms are tied to the flow regime via the densimetric Froude number Fr_d in overriding turbidity currents. This dimensionless number is defined as:

$$Fr_d = U/\sqrt{RCgH} \quad (1)$$

where H is an appropriate measure of turbidity current thickness, U is the layer-averaged flow velocity, g is the acceleration of gravity, C is the layer-averaged volume concentration of suspended sediment in turbidity currents ($C << 1$), and R is the submerged specific gravity of the sediment. Numerical results in Figure 5a–c outline a plausible scenario for evolution of the Northern channel in response to a continuous turbidity current. A 12-days duration period in this example is selected arbitrarily. Figure 5a reveals that sediment waves in the channel initially form as antidunes. As the flow persists, the upstream antidunes get reworked and the first cyclic step with a clearly visible internal hydraulic jump forms in the vicinity of the inflow boundary, i.e., slope top (Figure 5b). In time, more and more upstream-marching cyclic steps bounded by hydraulic jumps emerge, with antidunes in their toe (Figure 5c). Eventually, antidunes are fewer and fewer until only cyclic steps remain in case a turbidity current lasts long enough. The numerically-generated sequence in Figure 5a–c captures the evolution of the Northern channel by way of upper-flow-regime bedforms. This very scenario is likely applicable to bedforms in the remaining two channels (Central and Southern) on the prodelta slope.

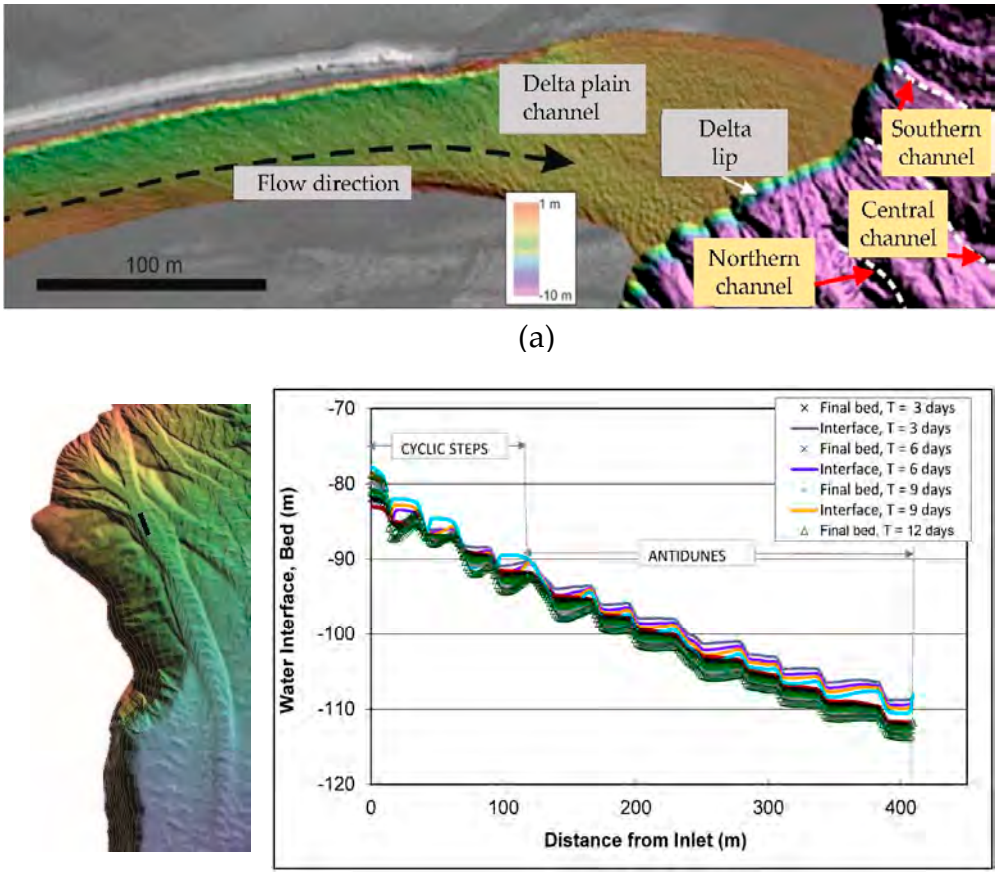

Figure 4. Squamish delta, British Columbia: (**a**) Top view shows the channelized delta plain and three incised channels (Northern, Central and Southern) on the steep prodelta slope (Adopted from Reference [70]). (**b**) Bedforms along the Northern channel (Adopted from Reference [70]). (**c**) Numerical results showing bed elevation and turbidity-current interface along the interpreted paleoslope profile shown in b (Adopted from Reference [23]).

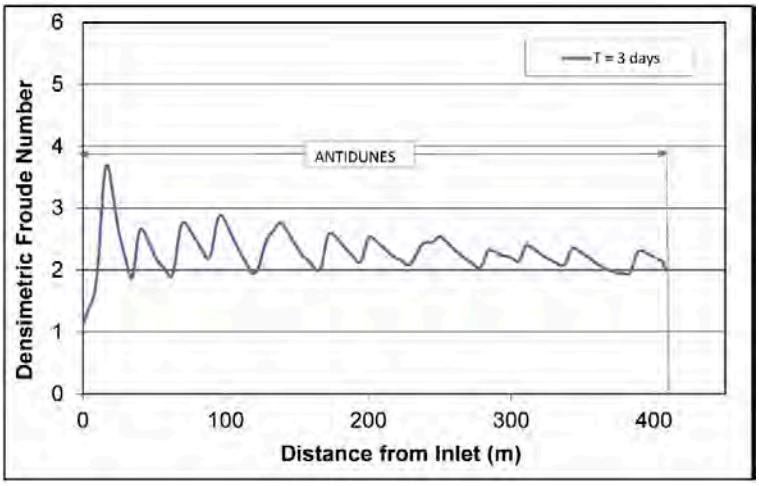

(**a**)

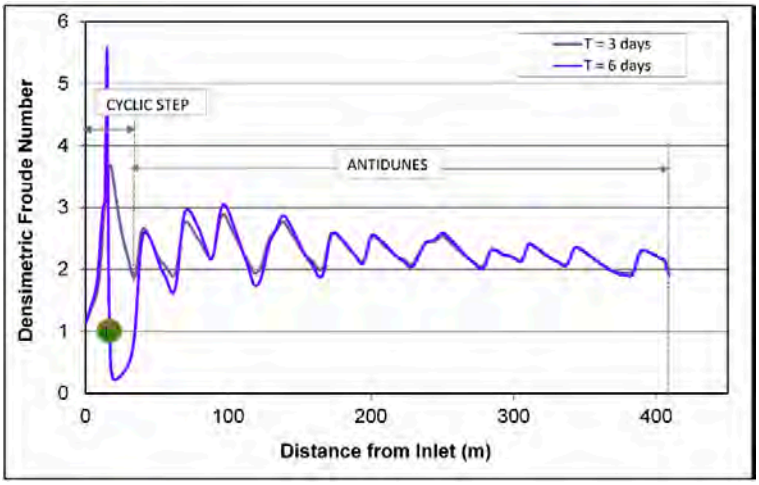

(**b**)

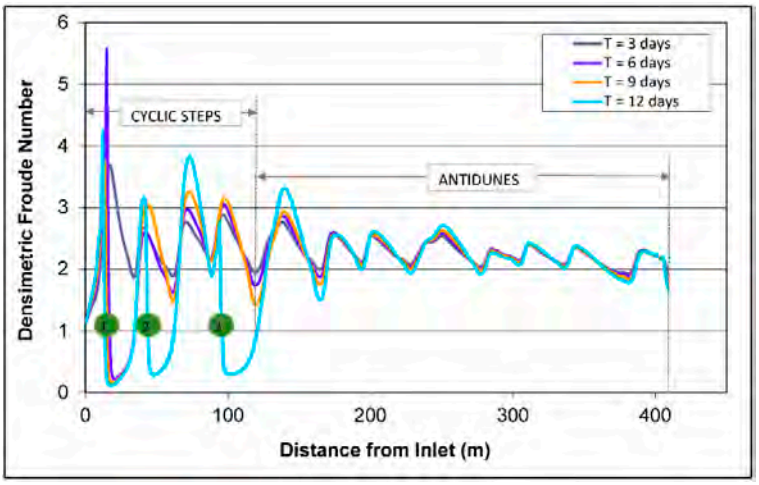

(**c**)

Figure 5. Plot of densimetric Froude number in the Northern channel: (**a**) Sediment waves form as antidunes. (**b**) First cyclic step emerges in time. (**c**) More antidunes get reworked into a train of upslope-marching cyclic steps after 12 days. Green circles in (**b**) and (**c**) show the location of internal hydraulic jumps.

2.3. What Was Learned from Numerical Experiments?

Unconfined sediment waves on selected Mediterranean deltas and confined crescent-shaped sediment waves within channels of the Squamish delta are similar to their counterparts on submarine fans in both process and form (e.g., References [18,20]). Only their wavelengths are at least an order of magnitude smaller than wavelengths of their deep-sea cousins. They can be classified as bedforms of intermediate wavelengths (roughly speaking $5 < L/H < 10$).

Extensive numerical experiments of Kostic [16] over a designed sloping bed consisting of sediment waves of intermediate wavelengths demonstrate that these features are likely to be transitional bedforms between antidunes and cyclic steps. Figure 6 summarizes one of the tests over a broad range of flow conditions; the incoming flow energy was varied considerably (*Frdo* = 3.52–0.79) by assigning values to the inflow depth (*Ho* = 50–1000 m). The details can be found in Reference [16].

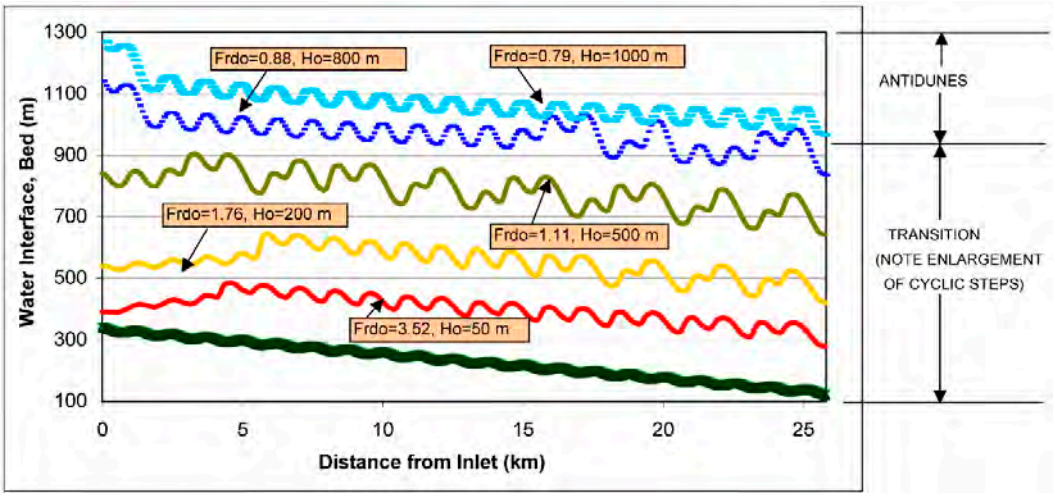

(**a**)

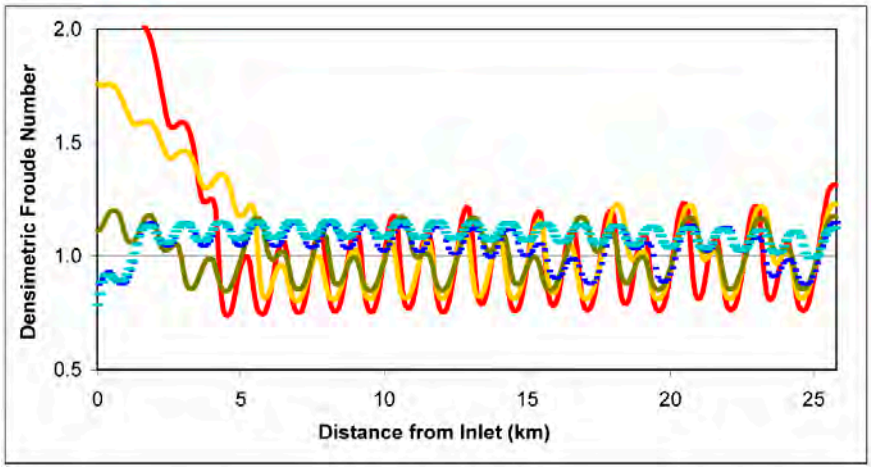

(**b**)

Figure 6. Hydrodynamic response of turbidity currents to intermediate-wavelength numerical sediment waves (Adopted from Reference [16]): (**a**) Bed and turbidity current interface profile for a range of inflow densimetric Froude number (*Frdo*) and assigned turbidity current inflow depths (*Ho*). (**b**) Corresponding plot of densimetric Froude number.

Transitional bedforms generated numerically in the example in Figure 6 include both end members of the family, i.e., stable antidunes (shown by teal line), and cyclic steps (shown by red line), as well as intermediate bedforms that represent a mix of both. A train of mixed bedforms with antidunes being

dominant (shown by blue line) is analogues to unstable antidunes observed in flume experiment on fluvial supercritical bedforms [71], whereas a train dominated by cyclic steps (shown by yellow line) would correspond to chutes-and-pools. Two distinctly different varieties of mixed upper-flow-regime bedforms deserve special attention: (a) Antidunes and cyclic steps within the same train (e.g., green and blue line), and (b) climbing antidunes superimposed on cyclic steps (upslope sections of red and yellow line). The results suggest that it is unlikely for submarine antidunes and cyclic steps of the same magnitude to form in a single train of sediment waves. Flume experiments [17] have also established that there was a gradual transition between antidunes and cyclic steps, and an order of magnitude difference in wavelengths between antidunes and cyclic steps within the same train.

Moreover, the results capture an important mechanism, which Kostic [16] named "enlargement". This mechanism involves merging of several smaller undulations into one bigger cyclic step, as shown in Figure 6. The process of enlargement possibly explains how the length difference between cyclic steps and antidunes comes into being and how sediment waves evolve through time. Field observations corroborate this finding. Sediment waves have been observed to sometimes merge upsection so that younger sections of a wave field have fewer yet larger individual waves than older sections [72,73]. The results in Figure 6 also suggest that the enlargement likely emanate from the downstream end of the flow field and travel upslope and upcurrent, likely due to the propagation direction of gravity waves in turbidity currents that form cyclic steps [16].

3. What Generates Cyclic Steps on Deltas?

Upstream-migrating antidunes are perhaps the best known bedforms of supercritical flows. In contrast, for a supercritical turbidity current to display internal hydraulic jumps that mold cyclic steps, the flow must decelerate from a supercritical region (where $Fr_d > 1$) toward a jump (where $Fr_d = 1$) and become subcritical (where $Fr_d < 1$). The presence of a slope break is a necessary, even though not a sufficient condition for the spontaneous evolution of an erodible plain bed into cyclic steps [15]. In Gilbert-type deltas, the foreset-bottomset break where a steep foreset deposit transitions into a nearly horizontal bottomset bed surely constitutes such a slope break (Figure 1).

A brief review of the comprehensive analysis presented in Reference [15] is provided below in order to show how the front-slope break facilitates the flow conditions conducive to cyclic steps. For the sake of simplicity, the governing physics behind internal hydraulic jumps in turbidity currents that mold cyclic steps is explained using the momentum equation only. The momentum equation for a steady, gradually varied turbidity current spreading in the longitudinal direction can be written as following [14]:

$$\frac{H}{U}\frac{dU}{dx} = \frac{S - e_w\left(Fr_d^2 + \frac{1}{2}\right) - c_f Fr_d^2 + \frac{1}{2} r_o \frac{v_s}{U}\left(1 - \frac{U e_s H}{r_o q}\right)}{Fr_d^2 - 1} \quad (2)$$

Here, x is a bed-attached streamwise coordinate, S is the streamwise bed slope, c_f is the bed friction coefficient, ro is a multiplicative constant, vs is the fall velocity of sediment, ew is the coefficient of water entrainment, and es is the coefficient of entrainment of bed sediment. The volume transport rate of suspended sediment per unit width q is defined as $q = HUC$.

For a supercritical turbidity current to undergo an internal hydraulic jump, the velocity U must decrease monotonically in x, or $dU/dx < 0$ in Equation (2). The denominator of the right-hand side of Equation (2) is positive for a supercritical flow. Therefore, the numerator of Equation (2) must be negative to render the formation of a hydraulic jump. The first term in the numerator denotes the driving force of gravity due to slope, the second and third term account for the interfacial and bed friction, respectively, while the last term represents the net deposition of sediment, i.e., deposition of suspended sediment on the bed reduced for erosion of bed sediment. The first and last term in Equation (2) act to suppress the ability of the flow to undergo a jump, whereas the third and fourth term promote the jump formation. This explains why a transition from a steep foreset to a nearly flat bottomset deposit in coarse-grained deltas acts to reduce the main force that opposes the jump

formation, i.e., streamwise pull of gravity. Furthermore, the fourth term in the numerator illustrates why the presence of a slope break is a necessary, but not a sufficient condition for the spontaneous evolution of an erodible plain bed into cyclic steps. If this term is overly large, as it is the case for highly-depositional turbidity currents, the condition $dU/dx < 0$ is not met and hydraulic jumps do not form [15]. Rather, these turbidity currents remain supercritical; they either thicken after the slope break, or die out upstream or downstream of the break due to rapid deposition. The cutoff size of sediment that causes turbidity currents to undergo internal hydraulic jumps can be linked to the ratio of the sediment fall velocity to inflow velocity vs/Uo [14]. Supercritical fine-grained turbidity currents that satisfy the approximate condition $vs/Uo < 3 \times 10^{-3}$ regularly display internal hydraulic jumps in response to a slope break, whereas coarse-grained currents with the ratio $vs/Uo > 5 \times 10^{-3}$ remain supercritical [14].

The foreset-bottomset break is not the only type of transition that can prompt internal hydraulic jumps in turbidity currents. Other triggers that have been recognized in the deep-water settings and may play a role in shallow-water environments include pre-existing bed perturbations [20] and transitions to areas of decreasing confinement [74]. Bed perturbations of one form or another (i.e., salt diapers, faults, paleo bedforms, etc.) are quite common on the seafloor. They promote the jump formation by decelerating supercritical flow via slope and bed friction in Equation (2). For example, rugose topography was found to be fundamentally important for nucleating cyclic steps in tectonically-active high-gradient submarine systems [20] where the downslope pull of gravity would ordinarily suppress the ability of the flow to undergo hydraulic jumps (Equation (2)). With this in mind, antidunes in Northern channel of the Squamish delta (Figure 5a) can be viewed as initial perturbations that, together with the foreset-bottomset break, promote the formation of cyclic steps in otherwise quite steep channel (Figure 5b,c). To understand the role of a transition to areas of decreasing confinement (e.g., canyon-fan transition, channel-lobe transition) in promoting hydraulic jumps, it is useful to revisit channel expansions in supercritical open-channel flow. These expansions frequently occur at places where flow emerges at high velocity from, e.g., a close conduit, spillway, sluice gate, or steep chute. If such expansions diverge too rapidly, the major part of the flow fails to follow the boundaries. As a result, flow separation was followed by eddies and shock waves that occurred [75]. By extension, energy losses due to flow separation at a transition to areas of decreasing confinement can facilitate the flow conditions conducive to a hydraulic jump and thus cyclic steps.

Furthermore, water and sediment inflow conditions likely play a significant role in generating cyclic steps on deltas. Thus, it is useful to summarize findings of several experiments on cyclicity in delta foreset bedding. Kleinhans [76] observed the formation of millimeter-scale cyclicity on delta foresets due to repeated events of sediment suspension at the mouth and grain flows. Events of sediment suspension at the mouth resulted in sedimentation of fine material near the foreset top, whereas grain flows preferentially moved coarser sediment toward the foreset toe. The experiment of Kim et al. [77] explored how a deltaic shoreline responds to changes in base-level under constant subsidence. They reported a pattern of delta foreset cyclic deposition linked to autogenically driven large-scale storage and release of sediment from the delta topset. Muto et al. [78] established that cyclic sedimentation of foreset deposit can be triggered by the periodic alternation between supercritical and subcritical flow on the delta topset just upstream of the shoreline. Distinct foreset undulations can be sustained as long as the inflow conditions of water and sediment support the formation of cyclic steps on the topset alluvial bed.

4. Field Case Study 1: Mazzarrà River Delta, Italy

4.1. Setting

The study area is located in the Gulf of Patti, in the NE part of Sicily, Italy (Figure 7). The onshore area is part of the Calabro-Peloritani arc, formed by a stack of crystalline, discontinuously overlied by Mesozoic limestones and Cenozoic flysch deposits [79,80]. The Gulf of Patti and its onshore sector

is a seismically very active region, with more than 2000 earthquakes recorded in the last 30 years, including the 6.1 Mw event in 1978 [81,82]. Most of the seismicity is related to the NNW–SSE trending right-lateral strike-slip "Aeolian–Tindari–Letojanni" fault system, interpreted as a lithospheric transfer zone [83]. The study area has been affected by uplift rates of 1–2 mm per year since the Pleistocene [84]. Due to this rapid uplift, the coastal range is carved by a network of short and steep rivers, locally named Fiumara [85]. Such rivers are dry during most of the year due to the semi-arid Mediterranean climate, but can get significant flows during flash floods in the autumn and winter months. The study area is characterized by the highest amount of rain per year in Sicily (between 700 and 1300 mm), because Peloritani Mountains act as a topographic barrier for the dominant and humid NW-wind from the Tyrrhenian Sea. During flash-flood events, a large volume of debris is transported into the sea. The flash floods often trigger hyperpycnal flows, as observed in the 2009 event in the nearby Western Messina Strait [86].

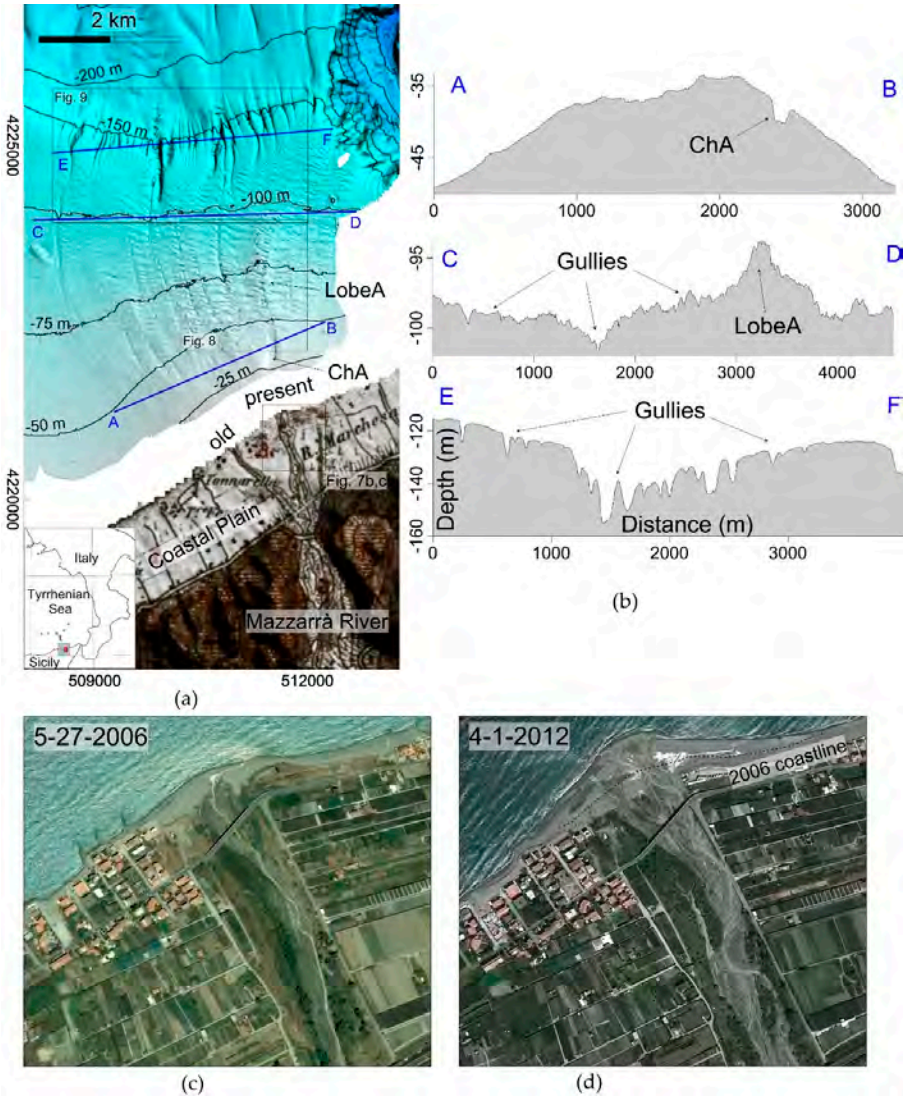

Figure 7. Field case 1: (**a**) Shaded relief map with isobaths (25-m equidistance) of the deltaic system offshore the Mazzarrà river mouth reveals unconfined and confined upper-flow-regime bedforms (NE Sicily; site location shown in the inset). Note that the 1884 geological map reveals two distinct channels at the river mouth. (**b**) Bathymetric profiles across the Mazzarrà delta at different water depths (blue lines in (**a**) show profile locations). (**c**) 2006 aerial photo of the present-day Mazzarrà fiumara mouth (downloaded from Google Earth). (**d**) Comparison with the 2012 image records the coastline progradation associated with a high-energy 2011 flash-flood event.

One of the main water courses debouching into the Gulf of Patti is the Mazzarrà river, which is credited with the formation of the deltaic system shown in Figure 7a,b. The Mazzarrà river drainage area encompasses 120 km^2 and has a maximum elevation of about 1200 m. Its course is about 25 km long, with slopes ranging from 25° in the upper reach to 0.3° in the 2 km wide coastal plain (the average slope is around 5°). Maximum river discharge is estimated to be between 500 and 780 m^3/s for the recurrence period of 50 and 300 years, respectively [87]. The drainage basin is largely affected by shallow instability processes occurring in strongly fractured basement rocks and flyschoid deposits, which can be easily remobilized during flash-flood events and can trigger the formation of mud/debris flows. A time lapse analysis of aerial photos for the period 2002–2014 has revealed the active coastal zone at the Mazzarrà river mouth. The documented progradation of the coastline between 2006 (Figure 7c) and 2012 (Figure 7d) is likely in response the 2011 flash-flood event. At a relatively longer timescale, a comparison of the 1884's and recent aerial photos shows that the Mazzarrà river mouth was previously formed by two main channels (Figure 7a), whereas it is confined within the main eastern channel since the 1960–1969 period (Figure 7c,d).

The facing offshore area is a relatively low-energy shelf area, dominated by storm waves with a maximum significant height of 3–4 m and a maximum tide of 0.6 m [88].

4.2. Materials and Methods

Marine geophysical data offshore Mazzarrà river mouth were collected during three oceanographic cruises performed in August 2011, January 2012, and December 2015 onboard R/V Urania and Minerva1 (National Research Council). Multibeam bathymetry was acquired at depths of -20/-300 m through a hull-mounted Kongsberg EM710 system working at a frequency of 70/100 kHz. Data were processed with Caris Hips and Sips 8.1 taking into account daily sound speed profiles and patch tests of transducers in areas close to the survey [48]. Statistical and geometrical filters were first applied for each swath in order to remove coherent/incoherent noise. Afterwards, a manual editing of spikes due to single fake soundings was performed. A Digital Terrain Model with the 5 m cell size was generated from processed data.

Single-channel seismic profiles were obtained with a hull-mounted Teledyne BENTHOS III CHIRP system operating with a frequency modulation of 2–20 kHz, which allowed for a 0.5 m vertical resolution. Seismic and multibeam data were positioned using differential GPS in order to reach a sub-metric accuracy on the x-y plane.

4.3. Results

4.3.1. Mazzarrà Deltaic System

The study area is characterized by a 6 km-wide continental shelf, which is dominated by a deltaic system of the Mazzarrà river extending down to -110 m (Figure 8). The surveyed Mazzarrà delta is limited coastward to the −25 m isobath and covers a surface of about 15 km^2; it shows an overall seaward-convex shape, with delta slope of 1°–3° (Figure 8a). The delta starts as a main convex lobe, evolving downslope in three overlapping and lobate areas, characterized by a progressive decrease in convexity both seaward and westward, where the seafloor tends to become flat (see bathymetric profiles A-B, C-D and E-F in Figure 7a,b). The overall delta morphology is quite rugged as it is dominated by unconfined sediment waves and shallow trains of scours within numerous gullies (Figure 8; Figure 9). The deltaic system is mainly composed of silty sediments (mean grain size D50 is between 9 and 30 μm), as documented by collected samples and backscatter images [48]. The exception are a few sandy samples recovered in the gullies carving the outer continental shelf/upper slope (D50 of 312 μm).

Seismic profiles reveal that the submarine deltaic system is being developed above an unconformity surface, which is interpreted as the erosive surface related to sub-aerial erosion following the last glacial sea level fall (at about 20 ka) and subsequent transgressive reworking (Figures 8b and

9b). The deltaic deposit forms a sedimentary wedge up to 50 m thick that can be divided into two main seismic units based on the geometry and characteristics (amplitude and continuity) of the seismic reflectors (Figures 8 and 9). The lower unit (SU1 in Figure 8b) is mainly characterized by transparent seismic facies and/or sub-parallel reflectors, and it can be split into different sub-units with onlapping geometries in cross-strike sections [48]. The upper unit (SU2 in Figure 8b) forms an overall progradational clinoform, characterized by high-amplitude and high-continuity reflectors. Here, the reflectors are often organized in wavy structures interrupted by semi-transparent layers.

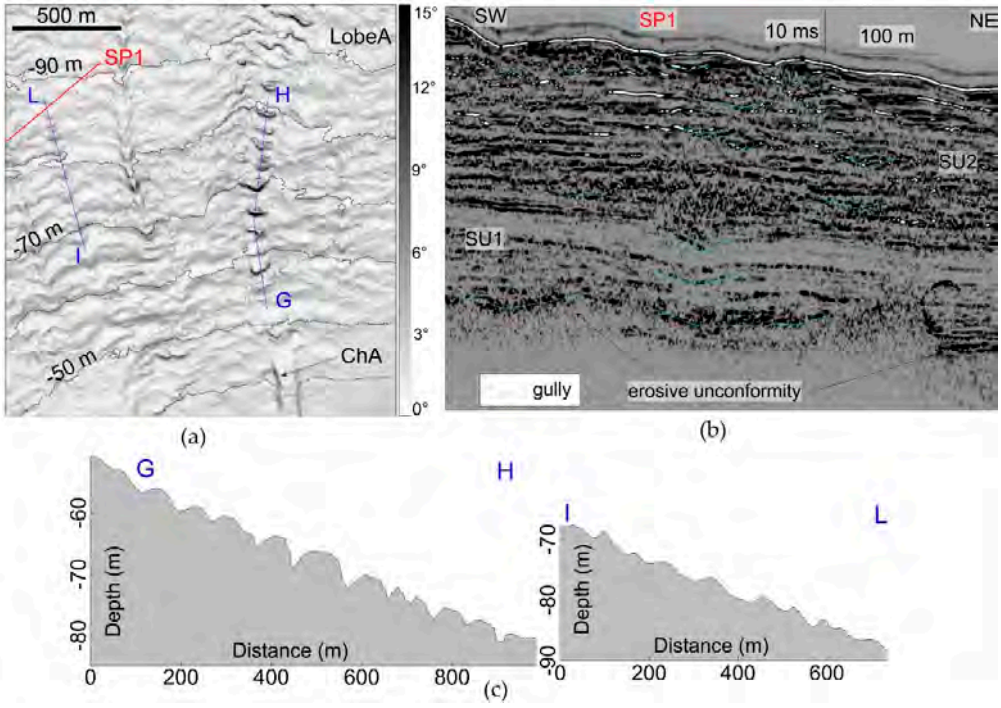

Figure 8. Proximal portion of the Mazzarrà prodelta: (**a**) Slope gradient map with isobaths (10-m equidistance) shows distinct unconfined sediment waves dissected by multiple gullies. A larger, U-shaped gully (ChA) is located just off the present-day river mouth; downslope of ChA is a main depositional lobe A with shallow channelized scours along the gully axis. (**b**) Chirp profile (location shown in (**a**) as a red line) illustrates the presence of an erosive unconformity overlaid by two seismic units SU1 and SU2 that made up the deltaic system; 10 ms denotes two-way travel time in milliseconds. Distinct V- and U-shaped erosive features can be interpreted as relict gullies. (**c**) Bathymetric profiles along confined bedforms (location shown in (**a**) as blue lines).

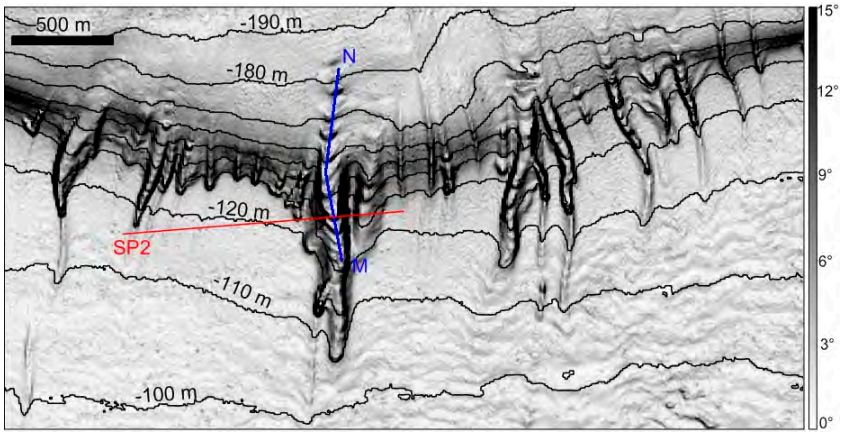

(**a**)

Figure 9. *Cont.*

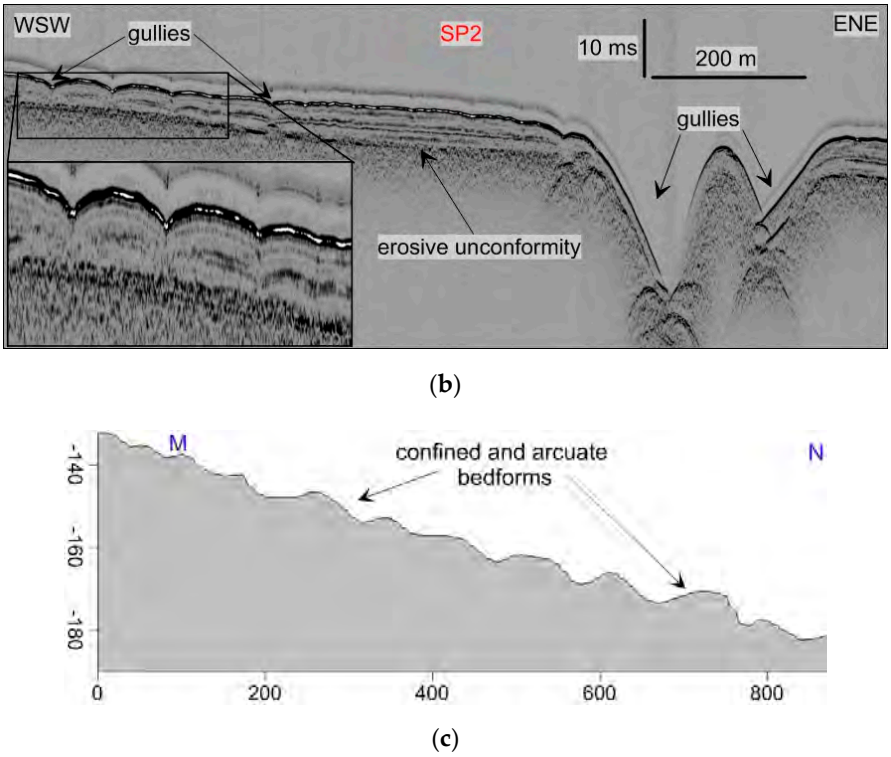

Figure 9. Distal portion of the Mazzarrà delta: (**a**) Slope gradient map with isobaths (10 m equidistance) illustrates that gullies with associated confined bedforms largely cut the outer shelf-upper slope. (**b**) The chirp profile (location shown in (**a**) as a red line) reveals shallow gullies on the left, which are confined in the sedimentary cover above the erosive unconformity. On the right, two markedly erosive gullies are present, largely cutting the basal unconformity. (**c**) Bathymetric profile (location shown in (**a**) as a blue line) along the thalweg of the main gully, revealing a coaxial train of bedforms.

4.3.2. Bedforms of the Mazzarrà Deltaic System

A variety of bedforms has been observed on the Mazzarrà delta, including unconfined wave-like bedforms, gullies and associated confined bedforms (Figure 7, Figure 8, Figure 9). Unconfined bedforms are ubiquitous between -50 m and -110 m and are characterized by sinuous or straight crest lines, oriented parallel to the isobaths. They display wavelengths L of 34 and 110 m and wave amplitudes A of 0.5 to 3 m (vertical form index L/A is 20–190, but mostly <100). They extend laterally for a few hundreds of meters. Wave dimensions tend to decrease in the distal part as well as moving westward in agreement with the minor convexity of the deltaic system (bathymetric cross-section in Figure 8). However, higher values of wave height are observed both in front of the historical and present-day river mouth, just off the channel A, where a main depositional lobe (Lobe A in Figure 7; Figure 8) is present.

Gullies are observed all along the deltaic system and in the upper slope. They vary in length (550–2440 m), width (80–300 m), and channel depth (0.3–3.5 m). In general, gullies are narrow and shallow on the shelf, while they increase in width and channel depth on the outer shelf-upper slope, where a marked increase in slope gradients is also present (Figure 9a). In a few cases, gullies eroded the erosive unconformity that delimits the base of the deltaic deposits (Figure 9b). Gullies are also observed in the sub-seafloor as relict features (light-blue lines in Figure 8b). The larger gullies are observed on the unconformity surface and just above it on the outer shelf; they decrease in number and size within the transparent units. A marked increase in number of gullies is observed in the upper stratigraphic levels, with a main concentration in the area between the two branches (present-day and historical) of the Mazzarà river mouth.

Bedforms along gullies are confined within their thalweg, generally displaying an arcuate or crescentic shape, always oriented perpendicular to the thalweg axis. They have wavelengths of 22–91 m and amplitudes of 0.5–4.5 m (vertical form index L/A is 14–48), whereas their lateral extent commonly matches the floor width of the hosting gullies. These features are often difficult to recognize in the shelf gullies, but they markedly increase in size in the gullies cutting the outer shelf-upper slope. In cross-sections, such bedforms commonly show a downslope asymmetry. Bedforms along gullies on Mazzarrà river delta are comparable in size and morphology to those observed in channels of the Squamish delta (Chapter 2.2) or at the head of the Monterey Canyon [89].

5. Field Case Study 2: Gilbert-Type Glaciolacustrine Deltas, Germany

5.1. Setting

The study area is located in Northern Germany (Figure 10). The blocking of river valleys by the Middle Pleistocene Scandinavian ice sheets (Marine Isotope Stages MIS 12–6) led to the repeated formation of numerous ice-dammed lakes ([51,90,91]). These steep ice-dammed lakes were characterized by overall lake-level rises during ice advances when lake-overspill channels were successively closed. Lake-level rises were up to 150 m within a few hundreds to thousands years. During deglaciation, the lakes catastrophically drained due to the renewed opening of lake outlets, which caused rapid, high-magnitude lake-level falls of the order of 20–65 m within a few weeks [92–94].

Figure 10. Location of the study area in northern Germany, showing the maximum extent of the Middle Pleistocene Elsterian and Saalian ice sheets in Central Europe and associated ice-marginal delta systems (Adopted from Reference [51]). Notation used for deltas is as follows: Be Betheln delta, Bo Bornhausen delta, C Coppenbrügge subaqueous fan and delta complex, E Emme delta, F Freden delta, G Großsteinberg delta, K Karsdorf delta, M Markendorf delta, P Porta subaqueous fan and delta complex, W Wünsch delta, Z Zeuchfeld delta.

5.2. Materials and Methods

Six ice-marginal delta systems selected for this study are considered to be representative of small Gilbert-type deltas, dominated by supercritical density flows. These deltas are referred to as Markendorf delta, Porta delta, Emme delta, Betheln delta, Freden delta, and Wünsch delta (M, P, E, Be, F, and W in Figure 10). The geomorphology of delta systems was mapped from high-resolution digital elevation models (10 m grid, vertical resolution: ±0.5 m) and partly reconstructed from old topographic maps (1901/1937) with Arc GIS software. The sedimentary facies were defined in the outcrops, noting grain size, bed thickness, bed contacts, bed geometry, internal sedimentary structures, and soft-sediment deformation structures. Photo mosaics of larger outcrops were used for the interpretation of architectural elements.

Ground-penetrating radar (GPR) and shear-wave seismic surveys were used to delineate architectural elements and to map the larger-scale delta architecture. Where possible, GPR and shear-wave seismic profiles were acquired next to outcrop walls to allow for a direct comparison between outcrop sections and the GPR and shear-wave seismic images. The GPR devices that have been used include a GSSI SIR-3000 and SIR-4000 GPR with 200 MHz, 400 MHz, and 1.5 GHz shielded antennas. Data processing comprised of dewowing, static correction, amplitude balancing by spherical divergence compensation, and application of an exponential gain function, bandpass filtering and migration. The vertical resolution for the 200 and 400 MHz antennas is ~5–10 cm. The lateral resolution is ~30–50 cm near the surface and ~0.8–1.1 m at 5 m depth. For the 1.5 GHz antenna the vertical resolution is ~4 cm and horizontal resolution ranges ~7–22 cm (0.1–1 m depth). Where possible, GPR sections were acquired next to outcrop walls to allow for a direct comparison between the GPR image and the outcrop section. The larger-scale delta architecture was mapped from high-resolution shear-wave seismic profiles. The seismic SH body wave type was used because it achieves up to 10 times higher resolution than P-wave seismic, resulting in a vertical resolution of ~0.5 m and a lateral resolution starting at 0.5 m near the surface and decreasing to approximately 12 m at 50 m depth. For all surveys presented here, a shear wave land streamer is combined with the micro-vibrator ELVIS, which operates in transverse horizontal (SH) mode, using a 20–160 Hz linear increasing sinusoidal sweep of 10-s duration as the seismic source signal. Seismic data processing focused on shear-wave velocity analysis after pre-processing of the raw data. The sedimentary facies and facies associations defined from outcrop analysis have been subsequently correlated with seismic units and geomorphology and then assigned to lake level. Additional details on data acquisition and processing of GPR and shear-wave seismic data can be found in References [51,93,95].

5.3. Results

5.3.1. Ice-Marginal Deltaic Systems

The ice-marginal Gilbert-type deltaic systems are relatively small, ranging in size from approximately 1.5 km^2 to 5 km^2. They display stair-stepped fan, tongue-shape or lobate geomorphologies and form ~35 m to ~70 m thick complexes. The Gilbert-type deltas are commonly located in front of mountain ranges or bedrock highs that acted as pinning points for ice lobes. In some cases, subaqueous ice-contact fans are downlapped, onlapped, or overlain by Gilbert-type delta systems [51,91].

Delta foresets have thicknesses between 5–30 m and foreset beds with slopes between 5°–34°. In strike sections, the foreset deposits form laterally and vertically stacked mounds, 15 to 360 m wide. Steeply dipping gravelly or sandy foreset beds either pass tangentially into relatively flat lying finer-grained bottomset facies or overlie bottomsets with an angular contact. In outcrops, the tops of foresets are commonly bounded by erosional surfaces and no topset-foreset transitions could be observed. Erosional surfaces are related to the formation of intermediate-wavelength bedforms, distributary channels or incised valleys. In seismic profiles foreset-topset transitions display rising sigmoidal, smooth-topped subhorizontal, or falling stepped-topped patterns [51].

The larger-scale depositional architecture of delta systems displays the typical stacking pattern of transgressive-regressive systems [96]. During glacial lake formation and overall transgression, vertically stacked delta bodies formed. The retrograding stair-stepped profiles of the transgressive delta systems indicate a rapid upslope shift of depocenters. During slowing rates of lake-level rise and lake-level highstands, accommodation space progressively decreased and the stratal stacking pattern changed from aggradation to progradation with subhorizontal or falling upper-delta-slope trajectories and an oblique erosional toplap geometry, which onlaps the inherited depositional profile. During high-magnitude lake-level falls, basinward stepping delta lobes formed that overlie and downlap the older landward-stepping delta bodies. Glaciofluvial incision led to erosion of the highstand deposits and the formation of deeply incised valleys. In front of these incised valleys coarse-grained forced regressive delta lobes with stepped-topped detached geometries formed. The deposition and upslope shift to finer-grained delta lobes indicates a decrease in flow velocity and sediment supply, probably related to increasing fluvial/delta plain aggradation in the incised valley during lake-level lowstand [93].

Stepped-topped attached sand-rich forced regressive aprons formed during lower magnitudes of lake-level falls or a rapid fall associated with a high sediment supply, causing only minor incision. Downslope, the sediment was supplied by relatively stable distributary channels over the older exposed delta plain [93]. If the remaining water depths during forced regression became low, coarse-grained shoal-water mouthbar deltas were deposited in front of the older Gilbert-type deltas [51].

5.3.2. Bedforms Emplaced by Supercritical Currents

The delta deposits include a large variety of sedimentary facies, representing deposition from low and high-energy tractional flows, debris flows, and sustained or surge-type supercritical to subcritical turbidity currents. Although the meltwater-source areas are likely to have yielded a significant fraction of silt and mud from glacial erosion the gravelly and sandy foresets are nearly devoid of silt and mud. The suspended load probably was mainly entrained in hypopycnal plumes and carried basinward. This sediment partitioning at the mouth of delta-feeder systems has been reported in other lacustrine and marine coarse-grained deltas and is characterized by the comparatively low thickness of bottomsets [51]. Flow velocities and sediment concentrations are difficult to estimate. Supercritical bedforms mainly occur in the sandrich delta foreset beds. Grain sizes commonly ranges between medium-grained sand to pebbly sand. Based on the foreset height, the water depths were between ~15 to 30 m. The frequent occurrence of climbing-ripple cross-lamination and dune-scale cross-stratification points to sustained flows and high rates of deposition.

(a) Bedforms emplaced by tractional supercritical currents: These bedforms are preserved in delta plain and upper delta slope deposits and comprise of isolated scour-fills and intermediate-wavelength bedforms (Figure 11). The intermediate wavelength bedforms consist of slightly asymmetric to symmetric sediment waves with wavelengths of ~60–90 m and amplitudes of ~3.8 to 5 m. In shear-wave seismic profiles, the wave-like structures are characterized by internal convex-up parallel high-amplitude reflectors. The slightly asymmetric bedforms have steeper upflow (stoss) slopes than the downflow (lee) slopes and pass downflow into more symmetrical bedforms. The estimated flow depth was ~9–14 m.

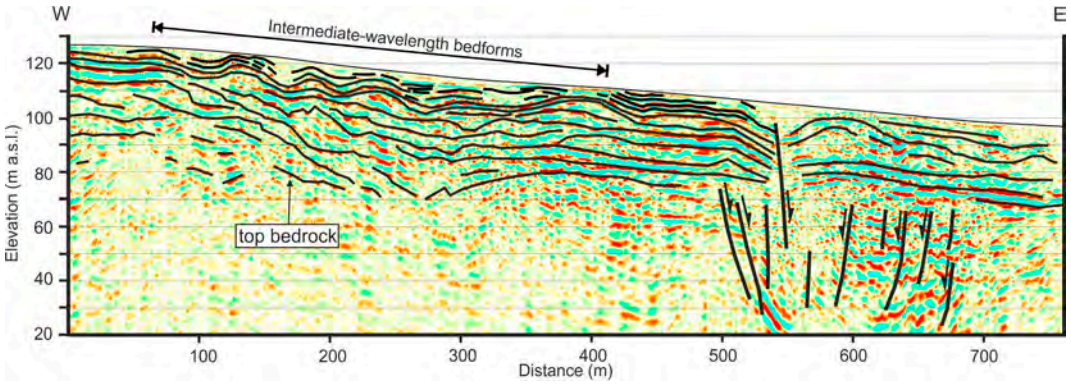

(**a**)

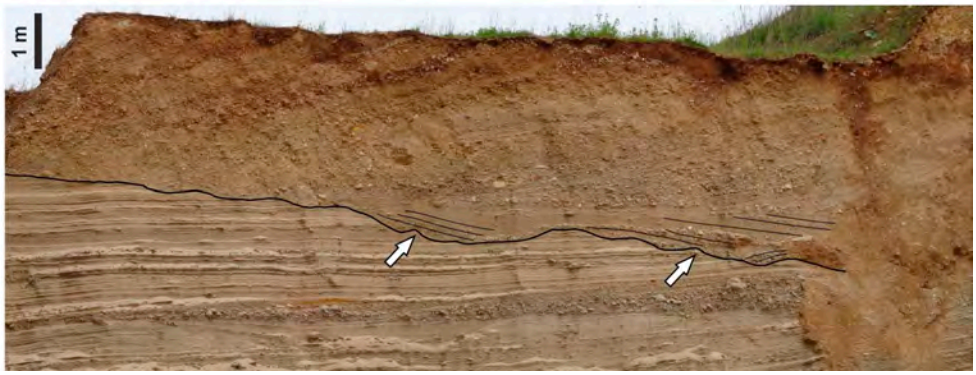

(**b**)

Figure 11. Bedforms emplaced by tractional supercritical currents: (**a**) Shear-wave seismic profiles of the Emme delta, showing intermediate-wavelength bedforms that developed on the delta plain and upper delta slope in front of an incised valley (Adopted from Reference [93]). (**b**) Isolated scour filled with backsets on top of truncated foreset beds (Betheln delta).

Bedforms with shorter wavelength of 38–45 m are associated with deep scours, filled with foresets. Based on their wavelengths and asymmetry, these deposits represent either large antidunes or net-depositional cyclic steps [93] or transitional upper-flow-regime bedforms [16].

(b) Bedforms emplaced by surge-type supercritical turbidity currents): Foreset beds, deposited by surge-type supercritical turbidity currents, comprise laterally and vertically stacked cyclic step and antidune deposits, which form meter-scale fining-upward sequences (Figure 12a). Individual foreset beds are 5 to 70 cm thick and consist of medium to coarse-grained sand, pebbly sand and gravel. Cyclic-step deposits are represented by lenticular scours, 0.9 m to more than 4 m long and 0.1 to 0.7 m deep. These scours are commonly isolated and widely spaced, have scooped basal erosional surfaces and are filled by backset cross-stratified pebbly sand and gravel. The gravelly scour fills commonly display an upslope dipping steep-clast fabric with no preferred orientation of the clast axes and fine upwards. Sandy scour fills may have a massive, diffusely graded or deformed basal part, passing upslope into backset cross-stratification. The soft-sediment deformation structures comprise convolute bedding, flame structures and clastic dykes. The scour fills are overlain by sheet-like, 5 to 15 cm thick beds of low-angle cross-stratified or sinusoidally stratified sand and pebbly sand, deposited from antidunes. The sheet-like beds commonly have erosional basal contacts and display frequent internal truncations and small-scale concave-up scours, but lateral transitions from the scour fills into the sheet-like beds are also observed. Locally, beds are draped by thin (0.5–1 cm) massive silty fine-grained sand layers. Upwards, the thickness of bedsets commonly increases and sigmoidally stratified pebbly sand occurs. The tops of the fining-upward successions are formed by thin beds (1–10 cm thick) of climbing ripple cross-laminated silty sand or massive silt and mud. The occurrence of isolated

cyclic-step deposits associated with antidune deposits may indicate deposition by waning turbidity currents at the lower limit of the cyclic-step stability field and the superimposition of antidunes on cyclic steps [16,22,95]. Alternatively, more isolated hydraulic-jump deposits may reflect rapidly decelerating and expanding low-efficiency flows, or short delta slopes, which prevent the re-establishment of supercritical flow conditions [97]. Drapes of silty fine-grained sand point to phases of suspension fall-out between the individual surges. The formation of dewatering structures in some scours indicates rapid suspension settling and pressure fluctuations in hydraulic-jump zones [98,99]. Lateral transitions from the scour fills into antidune deposits indicate the re-establishment of supercritical flow conditions on the stoss-sides of cyclic steps [95,100]. The occurrence of more extensive antidune deposits in some foreset beds points to temporarily relatively lower Froude numbers within the supercritical density flows [101]. Scouring within the antidune deposits may relate to antidune-wave breaking [71,102].

(c) Bedforms deposited from sustained supercritical turbidity currents: Foreset beds, deposited by sustained supercritical to subcritical turbidity currents are characterized by thick backsets and dune-scale foresets that occur over the entire delta foreset length (Figure 12b–g). These bedforms display little variation in thickness and grain size. Finer-grained silt or mud drapes are absent in this facies association. These delta-foreset deposits consist of medium to very thick-bedded sand and pebbly sand with laterally extensive trains of regularly spaced scour fills with asymmetrical geometries. Scours are 0.6 to 7 m long and 0.08 to 0.7 m deep and filled by backset cross-stratified pebbly sand. Backsets have concave-up, downflow divergent geometries and may display downflow transitions to convex-up or sigmoidal geometries. Perpendicular and oblique to palaeoflow these deposits appear as troughs, which are 1 to 5 m wide, up to 0.7 m deep and filled with concentric to low-angle cross-stratified pebbly sand. Backsets may display downflow transitions into sheet-like low-angle cross-stratified or sinusoidally stratified pebbly sand. Locally, foreset beds consist entirely of medium to thick-bedded low-angle cross-stratified or sinusoidally stratified pebbly sand. Finer-grained sandy foreset beds commonly display planar or trough cross-stratification. In the delta-toe zone of these foreset-bed packages sigmoidally cross-stratified sand is common. These humpback-dune deposits indicate less powerful transcritical sustained turbidity currents and highly aggradational conditions [71,102,103], probably related to a hydraulic jump at the basal break of slope [93]. The upward development from trough cross-stratified pebbly sand to preserved bedforms of finer-grained humpback dunes and antidunes may indicate flow thinning over aggrading beds leading to temporarily accelerating transcritical to supercritical flow conditions [71,102].

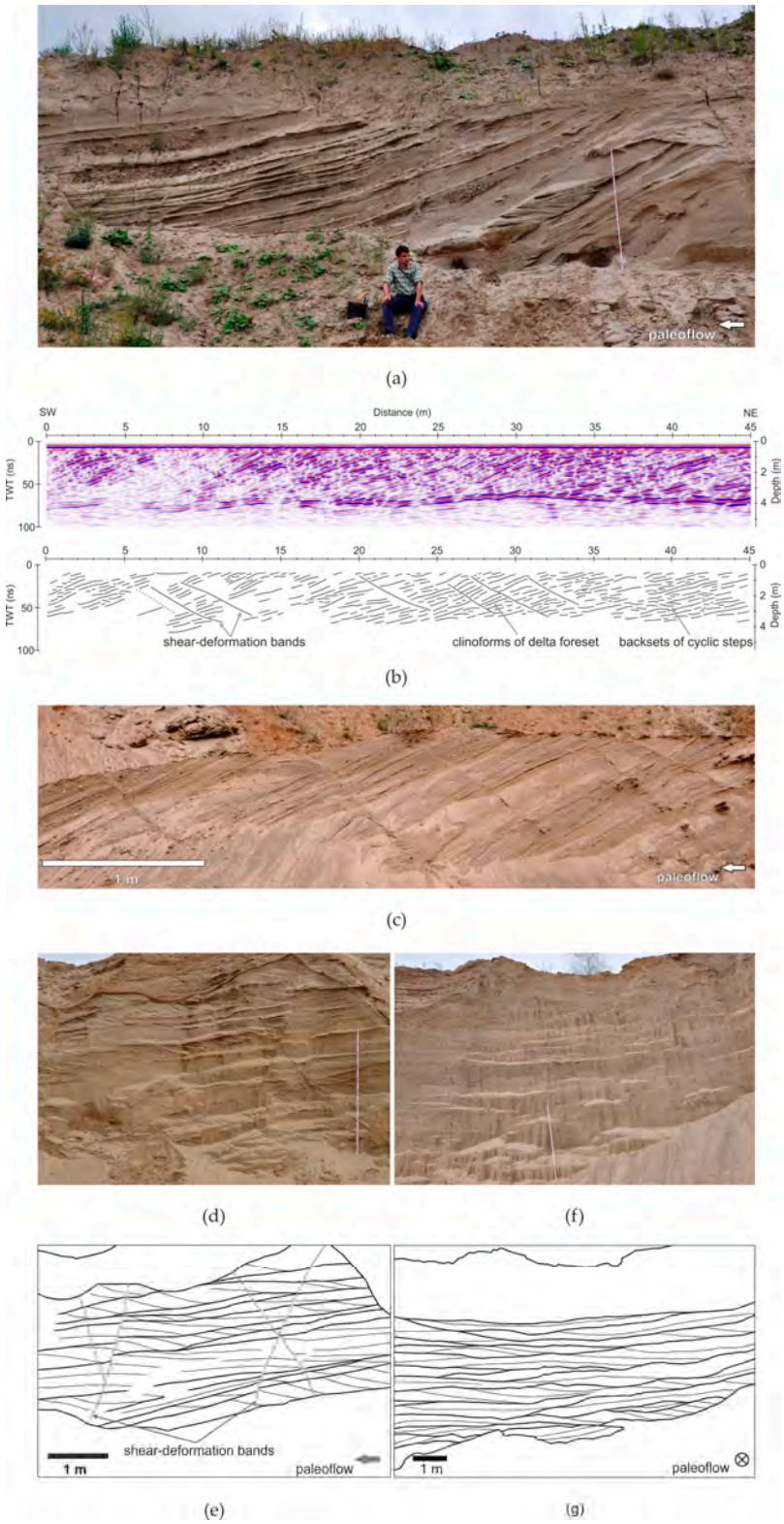

Figure 12. Sedimentary facies of delta foresets: (**a**) Sandy foreset beds, deposited from surge-type turbidity currents (Porta delta). (**b**–**g**) Sandy foreset beds, deposited from sustained turbidity currents (Freden delta), with (**b**) showing GPR profile (200 MHz); (**c**) showing outcrop analogue of lower delta foreset beds with backset cross-stratification and sigmoidal cross-stratification, displaced by shear deformation bands (Adopted from Reference [51]); and (**d**–**g**) showing photographs and line drawings of delta foreset beds with cyclic step and antidune deposits (Adopted from Reference [95]).

6. Discussion

Upper-flow-regime bedforms emplaced by supercritical sediment gravity flows have been recognized as crucial building blocks of deep-sea fans and canyon-channel systems [23]. These bedforms may also play an important role in the evolution of marine and lacustrine deltas as they appear to be much more common than previously though. They have been observed on marine and glaciolacustrine deltas in both unconfined and confined settings (marine deltas, e.g., Mediterranean deltas in Chapter 2.1., Mazzarrà delta in the Gulf of Patti in Italy in Chapter 4; Squamish delta in Chapter 2.2.; glaciolacustrine deltas: e.g., glaciolacustrine deltas in northern Germany in Chapter 5, [50]). In addition, contemporary and ancient upper-flow-regime bedforms have been recently recognized on deltas on Mars [104]. Contemporary upper-flow-regime bedforms on Martian deltas are attributed to the sporadic presence of flowing water on Mars.

Upper-flow-regime bedforms are transient, unstable features, which means that a slight increase in flow energy can trigger stable antidunes to transition into unstable antidunes, unstable antidunes into chutes-and-pools, and chutes-and-pools into cyclic steps. Therefore, their deposits are expected to display interbedding of their end members, i.e., cyclic steps and antidunes, as well as an intermediate bedforms that represent a superposition of both end members. More importantly, the presence of upper-flow-regime bedforms in deposits reveals that the formative sediment gravity flows fluctuate frequently and broadly. This is consistent with the main triggers for turbidity currents in river-fed systems (i.e., hyperpycnal river discharges [105,106], settling of sediment from hypopycnal plumes [105], and slope failures and sediment deformations [68,107] varying significantly in both energy and frequency.

The field case study of the Mazzarrà delta in the Gulf of Patti in Italy reveals trains of upper-flow-regime bedforms within gullies, which are dissecting sediment waves. Features confined with gullies are likely transitional upper-flow-regime bedforms instigated by uneven seafloor consisting of unconfined sediment waves [15,16] and possibly other trigger(s) discussed in Chapter 3. The Mazzarrà deltaic system with unconfined sediment waves and trains of scour-shaped depressions is in many ways similar and directly comparable to deep-sea systems such as the Monterey East system [18]. Only their wavelengths are at least an order of magnitude smaller than wavelengths of their deep-sea cousins, which make them intermediate-wavelength bedforms [16]. The morpho-stratigraphic data for the Mazzarrà delta suggest that hyperpycnal flows likely play a major role in the evolution of this system. The evidence of such high-energy events is the network of gullies branching at the river mouth. Similar gullies have been recognized off the mouth of other short and steep river in Sicily, e.g., Simeto and Niceto rivers [108,109], and Calabria, e.g., Mesima river [110], while they are mostly absent off the mouth of medium-size rivers in Italy. This is at least in part because short and steep torrential rivers are more prone to hyperpycnal flows during flash flood than large rivers [111]. On the other hand, recent research on the Squamish delta [70] recognized the role of settling from the riverine plumes and delayed delta-lip failures on the formation of turbidity currents in marine deltas. Delayed delta-lip failures that occurred hours after the flood peaks are attributed to cumulative delta plain sedimentation and tidally-induced pore pressure changes.

Upper-flow-regime bedforms in gullies are not limited to the surface of the deltaic system. They are also recognized in the sub-seafloor as relict erosive features. The gullies are mostly concentrated in the area between the two channel branches at the river mouth, which suggest that they are linked to riverine processes. Their temporal distribution also provides an insight into the relationship between riverine processes and sea-level fluctuations. For example, they are rather sparse in the lower seismic unit (SU1) that can be attributed to the transgressive system tract where the energy of riverine processes should be lower due to the rapid sea-level rise and the subsequent river base level. In contrast, gullies largely increase in number within the upper unit that has been emplaced during the highstand system tract, where a renewed progradation of a deltaic system occurs.

Gullies are generally shallow on the inner and middle shelf, whereas they markedly increase in size on the outer shelf-upper slope. This can likely be explained by growing erosive power of turbidity currents due to the marked increase of slope gradients at the shelf break.

Using the analogy with the deep-water systems [18,20], the narrow and shallow gullies and associated bedforms on the inner and middle shelf are interpreted as relatively young features, i.e., a sort of proto-channels, associated with sedimentary gravity flows due to the most recent flash-flood events. Similar features were recently observed off the Giampilieri Fiumara in the Western Messina Strait during the 2009 flash-flood event (e.g., Reference [86]). Alternatively, the low morphological relief of the shelf gullies could be attributed to the progressive infilling associated with the sedimentary dynamics acting on the delta. Such ongoing processes should completely fill these gullies in time, unless a new flash-flood generated turbidity current is able to re-erode the seafloor, exploiting the trace of these gullies.

It is worth noticing that the most prominent, U-shaped gully (ChA) is observed just off the present-day river mouth. The formation of this wider channel in contrast to other gullies could be explained by the anthropogenic confinement of the river in the main Eastern branch since the 1960s, which resulted in the recent focusing of the sedimentary gravity flows along this path. This could also explain the development of a depositional lobe at the end of this gully, which is the only lobe clearly detectible from the seafloor morphology. Moreover, an emerging proto-channel consisting of coaxial train of sinuous and arcuate upper-flow-regime bedforms is detected on the upper part of this lobe.

The field case study of glaciolacustrine deltas in northern Germany suggests that frequent occurrence of unconfined upper-flow regime bedforms on the delta foresets may be a typical feature of high-energy bedload-dominated feeder systems, which are characterized by steep delta slopes. These bedforms are particularly common in sand-rich glaciolacustrine delta deposits that formed during lake-level highstand and slow lake-level rise (Figure 13a,b). Supercritical density flows are most likely triggered by hyperpycnal meltwater flows and slope-failure events in response to accommodation changes on the delta plain.

During high-magnitudes of lake-level falls, deeply incised valleys form. Initial valley incision is probably caused by the formation of cyclic steps during rapid base-level fall. Intermediate-wavelength bedforms on the delta plain and upper delta slope provide evidence for incision by supercritical flows (Figure 13c). Coeval sediments of the delta-foot zone may be represented by thick sand beds with climbing dune stratification, which record high-energy turbulent waning flows under hydraulic-jump conditions during flow expansion at the mouth of the incised valley channel [93]. The incised valleys capture sediment and focus the sediment supply to coarse-grained regressive lobes in front of the incised valley, which leads to the development of digitate, tongue-shaped delta morphologies. These forced regressive deposits consist of sharp-based, high-angle foreset-bed packages (30°–10°). These packages are dominated by debris-flow deposits that correspond to strong fluvial erosion, leading to a related high sediment supply and en-mass deposition when the slope diminished [51,93].

During periods of slow lake-level rise when high rates of aggradation on the delta plain and in the upper slope zone occur, surge-type supercritical turbidity currents preferentially form. They are likely triggered by small-volume gravitational collapses of the upper delta slope. Shear-wave seismic profiles indicate that shoal-water mouthbar deposits on top of the delta plain are genetically linked to high-angle Gilbert-type foresets that are dominated by deposits of supercritical surge-type turbidity currents [51]. Meter-scale fining- and coarsening-upward trends may indicate seasonal or decanniel variations in meltwater flows and a related fluctuation of the lake-level and the delta-plain accommodation [51].

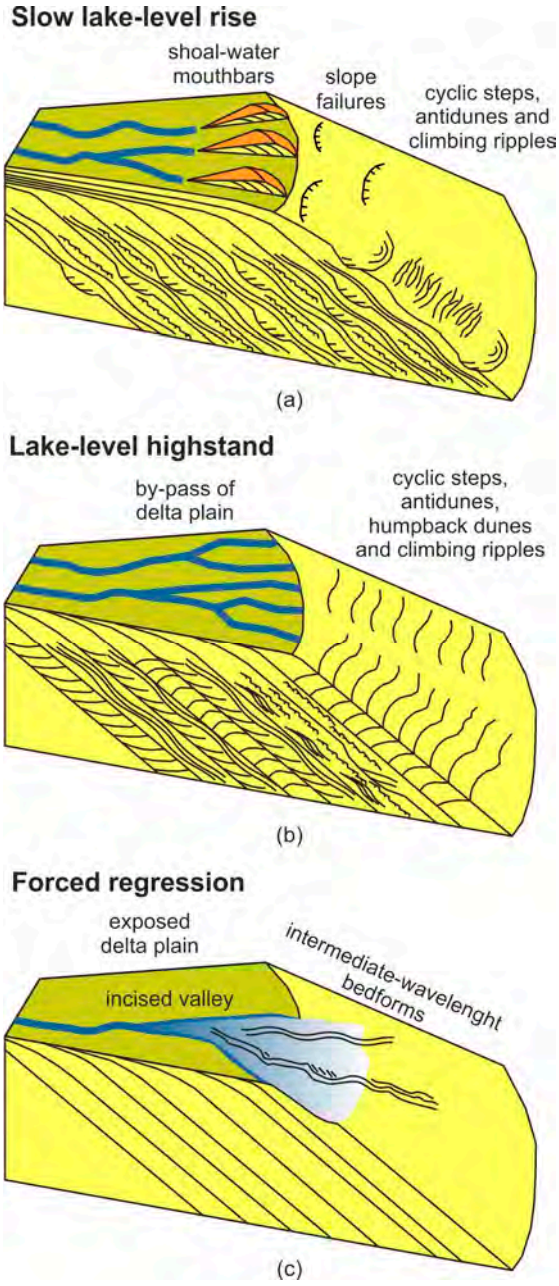

Figure 13. Schematic sketches of Gilbert-type deltas, showing characteristic bedforms, architectural features and stratal stacking patterns that developed during (**a**) slow lake-level rise, (**b**) lake-level highstand, and (**c**) forced regression. Modified from References [51,95].

During lake-level highstands more sustained supercritical turbidity currents are probably triggered by hyperpycnal plunging meltwater flows, when accommodation space in the upper-slope zone is reduced or at a minimum and a persistent sediment bypass of the delta plain occurs. Sediment concentrations in glaciofluvial systems are commonly high and flow densities exceed the ambient density of the glacial lakes. Flows from glaciofluvial feeder systems are thus likely to generate hyperpycnal flows that plunge over the upper delta slope [51,101,112,113]. These hyperpycnal flows can trigger the upslope migration of cyclic steps there and be sustained long enough to allow for the formation of migrating humpback dunes, dunes and climbing ripples on the lower delta slopes [51,95,114]. The frequent occurrence of upslope migrating climbing ripples may indicate the zone of flow transition of plane-wall jets emerging from the delta-plain channels [51,115]. These

supercritical systems are characterized by thick, high-angle foreset bedding, suggesting steep slopes with fan-shaped or lobate morphologies.

The common interbedding of cyclic-step and antidune deposits in successions related to sustained flows during lake-level highstands points to supercritical flow conditions with alternating Froude numbers. These changes in flow conditions may be related to variations in the meltwater discharge, which are subject to pronounced short-term and long-term variations, and rare extreme discharge events [25,116]. Furthermore, the formation of cyclic steps on the delta plain may trigger autogenic variations in discharge and sediment supply, which in turn can affect sediment deposition on the delta slope [78]. In transgressive systems that formed during slow lake-level rise, the interbedding of cyclic-step and antidune deposits is mainly related to waning surge-type flows triggered by slope failure events [51,95].

Author Contributions: S.K. proposed the topic, conceived the study, performed calculations, and wrote Chapters 1–4. D.C. and F.C. compiled the data for the Mazzarrà delta and wrote Chapter 5. J.L. and J.W. compiled the data for glaciolacustrine deltas in Germany and wrote Chapter 6. All authors contributed to Discussion (Chapter 7) and participated in several brain storming exchanges regarding the confusing delta terminology. Everyone read and approved the final manuscript.

Funding: This research is an invited review and received no external funding. S.K. acknowledges the JMSE editorial office for waving the publication fees.

Conflicts of Interest: The authors declare no conflict of interest.

References

1. Galloway, W.E. Process framework for describing the morphologic and stratigraphic evolution of deltaic depositional systems. In *Deltas, Models for Exploration*; Brousard, M.L., Ed.; Houston Geological Society: Houston, TX, USA, 1974; pp. 87–98.
2. Orton, G.J.; Reading, H.G. Variability of deltaic processes in terms of sediment supply, with particular emphasis on grain size. *Sedimentology* **1993**, *40*, 475–512. [CrossRef]
3. Postma, G. Depositional architectures and facies of river and fan deltas. In *Coarse-Grained Deltas*; Special Publication 10; Colella, A., Prior, D.B., Eds.; International Association of Sedimentologists, Blackwell Scientific Publications: Oxford, UK, 1990; pp. 13–27.
4. Gilbert, G.K. *Lake Bonneville*; Monography; U.S. Geological Survey: Washington, WA, USA, 1890; Volume 1, p. 438.
5. Fisk, H.N. Bar-finger sands of the Mississippi Delta. In *Geometry of Sandstone Bodies*; Peterson, J.A., Osmond, J.C., Eds.; American Association of Petroleum Geologists: Tulsa, OK, USA, 1961; pp. 29–52.
6. Holmes, A. *Principles of Physical Geology*; Thomas Nelson: London, UK, 1965; p. 1288.
7. Chough, S.K.; Hwang, I.G.; Choe, M.Y. The Miocene Domusan fan-delta, southeast Korea: A composite fan-delta system in back-arc margin. *J. Sediment. Petrol.* **1990**, *60*, 445–455.
8. Friedman, G.M.; Sanders, J.E.; Kopaska-Merkel, D.C. *Principles of Sedimentary Deposits—Stratigraphy and Sedimentology*; Macmillan: New York, NY, USA, 1992; p. 717.
9. Suter, J.R.; Berryhill, H.L. Late Quaternary shelf-margin deltas, northwest Gulf of Mexico: American Association of Petroleum Geologists. *AAPG Bull.* **1985**, *69*, 77–91.
10. Postma, G. Causes of architectural variation in deltas. In *Geology of Deltas*; Oti, M.N., Postma, G., Eds.; A.A. Balkema: Rotterdam, The Netherlands, 1995; pp. 3–16.
11. Kolla, V.; Biondi, P.; Long, B.; Fillon, R. Sequence stratigraphy and architecture of the late Pleistocene Lagniappe delta complex, northeast Gulf of Mexico. In *Sedimentary Responses to Forced Regressions*; Special Publication 172; Hunt, D., Gawthorpe, R.L., Eds.; Geological Society: London, UK, 2000; pp. 291–327.
12. Porebski, S.J.; Steel, R.J. Shelf-margin deltas: Their stratigraphic significance and relation to deep-water sands. *Earth-Sci. Rev.* **2003**, *62*, 283–326. [CrossRef]
13. Porebski, S.J.; Steel, R.J. Deltas and sea lever change. *J. Sediment. Res.* **2006**, *76*, 390. [CrossRef]
14. Kostic, S.; Parker, G. The response of turbidity currents to a canyon-fan transition: Internal hydraulic jumps and depositional signatures. *J. Hydraul. Res.* **2006**, *44*, 631–653. [CrossRef]

15. Kostic, S. Modeling of submarine cyclic steps: Controls on their formation, migration and architecture. *Geosphere* **2011**, *7*, 294–304. [CrossRef]
16. Kostic, S. Upper flow regime bedforms on levees and continental slopes: Turbidity current flow dynamics in response to fine-grained sediment waves. *Geosphere* **2014**, *10*, 1094–1103. [CrossRef]
17. Spinewine, B.; Sequeiros, O.E.; Garcia, M.H.; Beaubouef, R.T.; Sun, T.; Savoye, B.; Parker, G. Experiments on wedge-shaped deep sea sedimentary deposits in minibasins and/or on channel levees emplaced by turbidity currents. Part II. Morphodynamic evolution of the wedge and of the associated bedforms. *J. Sediment. Res.* **2009**, *79*, 608–628. [CrossRef]
18. Fildani, A.; Normark, W.R.; Kostic, S.; Parker, G. Channel formation by flow stripping: Large-scale scour features along the Monterey East Channel and their relation to sediment waves. *Sedimentology* **2006**, *53*, 1265–1287. [CrossRef]
19. Lamb, M.P.; Parsons, J.D.; Mullenbach, B.L.; Finlayson, D.P.; Orange, D.L.; Nittrouer, C.A. Evidence for superelevation, channel incision, and formation of cyclic steps by turbidity currents in Eel Canyon, California. *GSA Bull.* **2008**, *120*, 463–475. [CrossRef]
20. Covault, J.A.; Kostic, S.; Paull, C.K.; Rayan, H.F.; Fildani, A. Submarine channel initiation, filling and maintenance from seafloor geomorphology and morphodynamics modeling of cyclic steps. *Sedimentology* **2014**, *61*, 1031–1054. [CrossRef]
21. Symons, W.O.; Sumner, E.J.; Talling, P.J.; Cartigny, M.J.B.; Clare, M.A. Large-scale sediment waves and scours on the modern seafloor and their implications for the prevalence of supercritical flows. *Mar. Geol.* **2016**, *371*, 130–148. [CrossRef]
22. Lang, J.; Brandes, C.; Winsemann, J. Erosion and deposition by supercritical density flows during channel avulsion and backfilling: Field examples from coarse-grained deepwater channel-levee complexes (Sandino Forearc Basin, southern Central America). *Sediment. Geol.* **2017**, *349*, 79–102. [CrossRef]
23. Covault, J.A.; Kostic, S.; Paull, C.K.; Sylvester, Z.; Fildani, A. Cyclic Steps and Related Supercritical bedforms: Building Blocks of Submarine Fans and Canyon-Channel Systems, Western North America. *Mar. Geol.* **2017**, *393*, 4–20. [CrossRef]
24. Prior, D.B.; Bornhold, B.D. Submarine sedimentation on a developing Holocene fan delta. *Sedimentology* **1989**, *36*, 1053–1076. [CrossRef]
25. Gilbert, R.; Crookshanks, S. Sediment waves in a modern high-energy glacilacustrine environment. *Sedimentology* **2009**, *56*, 645–659. [CrossRef]
26. Urgeles, R.; Cattaneo, A.; Puig, P.; Liquete, C.; De Mol, B.; Amblas, B.; Sultan, N.; Trincardi, F. A review of undulated sediment features on Mediterranean prodeltas: Distinguishing sediment transport structures from sediment deformation. *Mar. Geophys. Res.* **2011**, *32*, 49–69. [CrossRef]
27. Gallignani, P. Recent sedimentation processes on the Calabrian continental shelf and slope (Tyrrenian Sea, Italy). *Oceanol. Acta* **1982**, *5*, 493–500.
28. Mougenot, D.; Buillot, G.; Rehault, J.P. Prograding shelf break types on passive margins: Some European examples. In *The Shelfbrak: Critical Interface on Continental Margins*; Stanley, D.J., Moore, G.T., Eds.; SEPM Special Publication: Tulsa, OK, USA, 1983; Volume 3, pp. 61–77.
29. Aksu, A.E.; Piper, D.J.W. Progradation of the late Quatrnary Gediz delta. *Mar. Geol.* **1983**, *54*, 1–25. [CrossRef]
30. Checa, A.; Dıaz, J.I.; Farran, M.; Maldonado, A. Sistemas deltaicos holocenos de los rıos Llobregat, Besos y Foix: Modelos evolutivos transgresivos. *Acta Geol. Hisp.* **1988**, *23*, 241–255.
31. Trincardi, F.; Normark, W.R. Sediment waves on the Tiber prodelta slope. *Geo-Mar. Lett.* **1988**, *8*, 149–157. [CrossRef]
32. Romagnoli, C.; Gabbianelli, G. Late Quaternary sedimentation and soft sediment deformation features in the Corigliano Basin. North Ionian Sea (Mediterranean). *Giornale di Geologia* **1990**, *52*, 33–53.
33. Ercilla, G.; Dıaz, J.I.; Alonso, B.; Farran, M. Late Pleistocene-Holocene sedimentary evolution of the northern Catalonia continental shelf (northwestern Mediterranean Sea). *Cont. Shelf Res.* **1995**, *15*, 1435–1451. [CrossRef]
34. Chiocci, F.L.; Esu, F.; Tommasi, P.; Chiappa, V. Stability of the submarine slope of the Tiber River delta. In *Landslides*; Senneset, K., Ed.; Balkema: Rotterdam, The Netherlands, 1996; pp. 521–526.
35. Correggiari, A.; Trincardi, F.; Langone, L.; Roveri, M. Styles of failure in late Holocene highstand prodelta wedges on the Adriatic shelf. *J. Sediment. Res.* **2001**, *71*, 218–236. [CrossRef]

36. Marsset, T.; Marsset, B.; Thomas, Y.; Cochonat, P.; Cattaneo, A.; Tricardi, F. Analysis of Holocene sedimentary features on the Adriatic shelf from 3D very high resolution seismic data (Triad survey). *Mar. Geol.* **2004**, *213*, 73–89. [CrossRef]
37. Cattaneo, A.; Correggiari, A.; Marsset, T.; Thomas, Y.; Marsset, B.; Trincardi, F. Seafloor undulation pattern on the Adriatic shelf and comparison to deep-water sediment waves. *Mar. Geol.* **2004**, *213*, 121–148. [CrossRef]
38. Fernandez-Salas, L.M.; Lobo, F.J.; Sanz, J.L.; Diaz-del-Rio, V.; Garcia, M.C.; Moreno, I. Morphometric analysis and genetic implications of pro-deltaic sea-floor undulations in the northern Alboran Sea margin, western Mediterranean Basin. *Mar. Geol.* **2007**, *243*, 31–56. [CrossRef]
39. Urgeles, R.; De Mol, B.; Liquete, C.; Canals, M.; De Batist, M.; Hughes-Clarke, J.E.; Amblas, D.; Arnau, P.A.; Calafat, A.M.; Casamor, J.L.; et al. Sediment undulations on the Llobregat prodelta: Signs of early slope instability or bottom current activity? *J. Geophys. Res.* **2007**, *112*. [CrossRef]
40. Lykousis, V.; Roussakis, G.; Sakellariou, D. Slope failures and stability analysis of shallow water prodeltas in the active margins of Western Greece, northeastern Mediterranean Sea. *Int. J. Earth Sci.* **2009**, *98*, 807–822. [CrossRef]
41. Agate, M.; Di Grigoli, G.; Lo Iacono, C.; Lo Presti, V.; Mancuso, M.; Sulli, A.; Vaccaro, F. Decoding the instabilities features along the continental margin of Sicily (central Mediterranean Sea. *Soc. Geol.* **2009**, *7*, 99–101.
42. Rebesco, M.; Neagu, R.C.; Cuppari, A.; Muto, A.; Accettella, D.; Dominici, R.; Cova, A.; Romano, C.; Caburlotto, A. Morphobathymetric analysis and evidence of submarine mass movements in the western Gulf of Taranto (Calabria margin, Ionian Sea). *Int. J. Earth Sci.* **2009**, *98*, 791–805. [CrossRef]
43. Kostic, S.; Parker, G. Progradational sand-mud deltas in lakes and reservoirs, Part 2. Experiment and numerical simulation. *J. Hydraul. Res.* **2003**, *41*, 141–152. [CrossRef]
44. Trincardi, F.; Cattaneo, A.; Correggiari, A. Mediterranean prodelta systems: Natural evolution and human impact investigated by EURODELTA. *Oceanography* **2004**, *17*, 34–45. [CrossRef]
45. Hughes Clarke, J.E.; Brucker, S.; Muggah, J.; Church, I.; Cartwright, D.; Kuus, P.; Hamilton, T.; Pratomo, D.; Eisan, B. The Squamish ProDelta: Monitoring active landslides and turbidity currents. In Proceedings of the Canadian Hydrographic Conference, Niagara Falls, ON, Canada, 15–17 May 2012; Volume 15.
46. Hughes Clarke, J.E.; Vidiera Marques, C.R.; Pratomo, D. Imaging active mass-wasting and sediment flows on a fjord delta, Squamish, British Columbia. In *Submarine Mass Movements and Their Consequences*; Advances in Natural and Technological Hazards Research; Krastel, S., Behrmann, J.H., Völker, D., Stipp, M., Berndt, C., Eds.; Springer: Cham, Switzerland, 2014; Volume 37, pp. 249–260.
47. Hughes Clarke, J.E. First wide-angle view of channelized turbidity currents links migrating cyclic steps to flow characteristics. *Nat. Commun.* **2016**, *7*, 11896. [CrossRef]
48. Casalbore, D.; Ridente, D.; Bosman, A.; Chiocci, F.L. Depositional and erosional bedforms in Late Pleistocene-Holocene pro-delta deposits of the Gulf of Patti (southern Tyrrhenian margin, Italy). *Mar. Geol.* **2017**, *385*, 216–227. [CrossRef]
49. Fricke, A.T.; Sheets, B.A.; Nittrouer, C.A.; Allison, M.A.; Ogston, A.S. An examination of Froude-supercritical flows and cyclic steps on a subaqueous Lacustrine delta, Lake Chelan, Washington, USA. *J. Sediment. Res.* **2015**, *85*, 754–767. [CrossRef]
50. Normandeau, A.; Lajeunesse, P.; Poiré, A.G.; Francus, P. Morphological expression of bedforms formed by supercritical sediment density flows in four fjord-lake deltas of the southeastern Canadian Shield (Eastern Canada). *Sedimentology* **2016**, *63*, 2106–2129. [CrossRef]
51. Winsemann, J.; Lang, J.; Polom, U.; Loewer, M.; Igel, J.; Pollock, L.; Brandes, C. Ice-marginal forced-regressive deltas in glacial lake basins: Geomorphology, facies variability and large-scale depositional architecture. *Boreas* **2018**, *47*, 973–1002. [CrossRef]
52. Cattaneo, A.; Trincardi, F.; Asioli, A.; Correggiari, A. The western Adriatic shelf clinoform: Energy-limited bottomset. *Cont. Shelf Res.* **2007**, *27*, 506–525. [CrossRef]
53. Dıaz, J.I.; Ercilla, G. Holocene depositional history of the Fluvia-Muga prodelta, northwestern Mediterranean Sea. *Mar. Geol.* **1993**, *111*, 83–92. [CrossRef]
54. Puig, P.; Ogston, A.S.; Guillen, J.; Fain, A.M.V.; Palanques, A. Sediment transport processes from the topset to the foreset of a crenulated clinoform (Adriatic Sea). *Cont. Shelf Res.* **2007**, *27*, 452–474. [CrossRef]

55. Sultan, N.; Cochonat, P.; Canals, M.; Cattaneo, A.; Dennielou, B.; Haflidason, H.; Laberg, J.S.; Long, D.; Mienert, J.; Trincardi, F.; et al. Triggering mechanisms of slope instability processes and sediment failures on continental margins: A geotechnical approach. *Mar. Geol.* **2004**, *213*, 291–321. [CrossRef]
56. Sultan, N.; Cattaneo, A.; Urgeles, R.; Lee, H.; Locat, J.; Trincardi, F.; Berne, S.; Canals, M.; Lafuerza, S. A geomechanical approach for the genesis of sediment undulations on the Adriatic shelf. *Geochem. Geophys. Geosyst.* **2008**, *9*. [CrossRef]
57. Milliman, J.D.; Syvitski, J.P.M. Geomorphic/tectonic control of sediment discharge to the ocean: The importance of small mountainous rivers. *J. Geol.* **1992**, *100*, 525–544. [CrossRef]
58. Syvitsky, J.P.M.; Kettner, A.J. On the flux of water and sediment into the Northern Adriatic Sea. *Cont. Shelf Res.* **2007**, *27*, 296–308. [CrossRef]
59. Liquete, C.; Arnau, P.; Canals, M.; Colas, S. Mediterranean river systems of Andalusia, southern Spain, and associated deltas: A source to sink approach. *Mar. Geol.* **2005**, *222–223*, 471–495. [CrossRef]
60. Benito, G.; Thorndycraft, V.R.; Rico, M.; Sanchez-Moya, Y.; Sopena, A. Palaeoflood and floodplain records from Spain: Evidence for long-term climate variability and environmental changes. *Geomorphology* **2008**, *101*, 68–77. [CrossRef]
61. Thorndycraft, V.R.; Benito, G.; Rico, M.; Sopena, A.; Sanchez-Moya, Y.; Casas, A. A long-term flood discharge record derived from slack-water flood deposits of the Llobregat River, NE Spain. *J. Hydrol.* **2005**, *313*, 16–31. [CrossRef]
62. Wheatcroft, R.A.; Stevens, A.W.; Hunt, L.M.; Milligan, T.G. The large-scale distribution and internal geometry of the fall 2000 Po river flood deposit: Evidence from digital X-radiography. *Cont. Shelf Res.* **2006**, *26*, 499–516. [CrossRef]
63. Demestre, M.; Guillen, J.; Maynou, F.; Palanques, A.; Puig, P.; Recasens, L.; Sanchez, P.; Belzunces, M.; Bucci, A.; Cruz, A.; et al. Estimacion del Impacto de las Obras del Plan Director Sobre los Recursos Pesqueros que Explota la Flota Pesquera de la Cofradıa de Barcelona. *Tech. Rep.* **2004**, 302.
64. Farrell, G.J.; Stefan, H.G. Mathematical modeling of plunging reservoir flows. *J. Hydraul. Res.* **1988**, *26*, 525–537. [CrossRef]
65. Ludwig, W.; Dumont, E.; Meybeck, M.; Heussner, S. River discharges of water and nutrients to the Mediterranean and Black Sea: Major drivers for ecosystem changes during past and future decades? *Prog. Oceanogr.* **2009**, *80*, 199–217. [CrossRef]
66. Syvitski, J.P.M.; Kettner, A.J.; Overeem, I.; Hutton, E.W.H.; Hannon, M.T.; Brakenridge, R.; Day, J.; Vörösmarty, C.J.; Saito, Y.; Giosan, L.; et al. Sinking deltas due to human activities. *Nat. Geosci.* **2009**, *2*, 681–686. [CrossRef]
67. Kostic, S.; Stefanovic, D. Flood-Control Levees on River Deltas: What We Have Learned from the New Orleans Hurricane Katrina Experience. In *Advances in Environmental Research*; Nova Science Publishers Inc.: Hauppauge, NY, USA, 2017; Volume 56, pp. 29–48.
68. Prior, D.B.; Bornhold, B.D.; Wiseman, W.J.; Lowe, D.R. Turbidity current activity in a British Columbia fjord. *Science* **1987**, *237*, 1330–1333. [CrossRef]
69. University of New Brunswick, Ocean Mapping Group. Squamish Prodelta Experiment. 2011. Available online: http://www.omg.unb.ca/Projects/SQ_2011_html/ (accessed on 20 November 2018).
70. Clare, M.A.; HughesClarke, J.E.; Talling, P.J.; Cartigny, M.J.B.; Pratomo, D.G. Preconditioning and triggering of offshore slope failures and turbidity currents revealed by most detailed monitoring yet at a fjord-head delta. *Earth Planet. Sci. Lett.* **2016**, *450*, 208–220. [CrossRef]
71. Cartigny, M.J.B.; Ventra, D.; Postma, G.; van den Berg, J.H. Morphodynamics and sedimentary structures of bedforms under supercritical-flow conditions: New insights from flume experiments. *Sedimentology* **2014**, *61*, 712–748. [CrossRef]
72. Carter, L.; Carter, R.M.; Nelson, C.S.; Fulthorpe, C.S.; Neil, H.L. Evolution of Pliocene to recent abyssal sediment waves on Bounty Channel levees, New Zealand. *Mar. Geol.* **1990**, *95*, 97–109. [CrossRef]
73. Ercilla, G.; Wynn, R.B.; Alonso, B.; Baraza, J. Initiation and evolution of turbidity current sediment waves in the Magdalena Turbidite System. *Mar. Geol.* **2002**, *192*, 153–169. [CrossRef]
74. Pemberton, E.A.L.; Hubbard, S.M.; Fildani, A.; Romans, B.; Stright, L. The stratigraphic expression of decreasing confinement along a deep-water routing sediment system: Outcrop example from southern Chile. *Geosphere* **2016**, *12*, 114–134. [CrossRef]
75. Hom-Ma, M.; Shima, S. On the flow in a gradually diverged open channel. *Jpn. Sci. Rev.* **1952**, *2*, 326–346.

76. Kleinhans, M.G. Autogenic cyclicity of foreset sorting in experimental Gilbert-type deltas. *Sediment. Geol.* **2005**, *181*, 215–224. [CrossRef]
77. Kim, W.; Paola, C.; Swenson, J.B.; Voller, V.R. Shoreline response to autogenic processes of sediment storage and release in the fluvial system. *J. Geophys. Res.* **2006**, *111*, F04013. [CrossRef]
78. Muto, T.; Yamagishi, C.; Sekiguchi, T.; Yokokawa, M.; Parker, G. The hydraulic autogenesis of distinct cyclicity in delta foreset bedding: Flume experiments. *J. Sediment. Res.* **2012**, *82*, 545–558. [CrossRef]
79. Ogniben, L. Schema introduttivo alla geologia del confine calabro-lucano. *Memorie della Società Geologica Italiana* **1969**, *8*, 453–763.
80. Lentini, F.; Carbone, S.; Guarnieri, P. Collisional and post-collisional tectonics of the Apenninic-Maghrebian Orogen (Southern Italy). In *Postcollisional Tectonics and Magmatism in the Eastern Mediterranean Region*; Special Paper; Dilek, Y., Pavlides, S., Eds.; Geological Society of America: Washington, WA, USA, 2006; Volume 409, pp. 57–81.
81. CPTI Working Group. Catalogo Parametrico dei Terremoti Italiani, Version 2004 (CPTI04). INGV: Bologna, Italy. Available online: http://emidius.mi.ingv.it/CPTI (accessed on 20 November 2018).
82. Chiarabba, C.; Jovane, L.; DiStefano, R. A new view of Italian seismicity using 20 years of instrumental recordings. *Tectonophysics* **2005**, *395*, 251–268. [CrossRef]
83. Cultrera, F.; Barreca, G.; Ferranti, L.; Monaco, C.; Pepe, F.; Passaro, S.; Barberi, G.; Bruno, V.; Burrato, P.; Mattia, M.; et al. Structural architecture and active deformation pattern in the northern sector of the Aeolian-Tindari-Letojanni fault system (SE Tyrrhenian Sea-NE Sicily) from integrated analysis of field, marine geophysical, seismological and geodetic data. *Ital. J. Geosci.* **2017**, *136*, 399–417. [CrossRef]
84. Sulli, A.; Lo Presti, V.; Gasparo Morticelli, M.; Antonioli, F. Vertical movements in NE Sicily and its offshore: Outcome of tectonic uplift during the last 125 ky. *Quat. Int.* **2013**, *288*, 168–182. [CrossRef]
85. Sabato, L.; Tropeano, M. Fiumara: A kind of high hazard river. *Phys. Chem. Earth A/B/C* **2004**, *29*, 707–715. [CrossRef]
86. Casalbore, D.; Chiocci, F.L.; Scarascia Mugnozza, G.; Tommasi, P.; Sposato, A. Flash-flood hyperpycnal flows generating shallow-water landslides at Fiumara mouths in Western Messina Straits (Italy). *Mar. Geophys. Res.* **2011**, *32*, 257–271. [CrossRef]
87. Hydro-geological Characterization of the Mazzarrà River Course. Available online: http://www.sitr.regione.sicilia.it/pai/bacini.htm (accessed on 20 November 2018).
88. Istituto Idrografico della Marina. *Atlante delle Correnti Superficiali dei Mari d'Italia*, 1st ed.; Istituto Idrografico della Marina no. 3068: Genova, Italy, 1982.
89. Paull, C.K.; Ussler, I.I.I.W.; Caress, D.W.; Lundsten, E.; Barry, J.; Covault, J.A.; Maier, K.L.; Xu, J.P.; Augenstein, S. Origins of large crescent-shaped bedforms within the axial channel of Monterey Canyon. *Geosphere* **2010**, *6*, 755–774. [CrossRef]
90. Roskosch, J.; Winsemann, J.; Polom, U.; Brandes, C.; Tsukamoto, S.; Weitkamp, A.; Bartholomäus, W.A.; Henningsen, D.; Frechen, M. Luminescence dating of ice-marginal deposits in northern Germany: Evidence for repeated glaciations during the Middle Pleistocene (MIS 12 to MIS 6). *Boreas* **2015**, *44*, 103–126. [CrossRef]
91. Lang, J.; Lauer, T.; Winsemann, J. New age constraints for the Saalian glaciation in northern central Europe: Implications for the extent of ice sheets and related proglacial lake systems. *Quat. Sci. Rev.* **2018**, *180*, 240–259. [CrossRef]
92. Meinsen, J.; Winsemann, J.; Weitkamp, A.; Landmeyer, N.; Lenz, A.; Dölling, A. Middle Pleistocene (Saalian) lake outburst floods in the Münsterland Embayment (NW Germany): Impacts and magnitudes. *Quat. Sci. Rev.* **2011**, *30*, 2597–2625. [CrossRef]
93. Winsemann, J.; Brandes, C.; Polom, U. Response of a proglacial delta to rapid high-amplitude lake level change: An integration of outcrop data and high resolution shear wave seismic. *Basin Res.* **2011**, *23*, 22–52. [CrossRef]
94. Winsemann, J.; Alho, P.; Laamanen, L.; Goseberg, N.; Lang, J.; Klostermann, J. Flow dynamics, sedimentation and erosion of glacial lake outburst floods along the Middle Pleistocene Scandinavian ice sheet (northern Central Europe). *Boreas* **2016**, *45*, 260–283. [CrossRef]
95. Lang, J.; Sievers, J.; Loewer, M.; Igel, J.; Winsemann, J. 3D architecture of cyclic step and antidune deposits in glacigenic subaqueous fan and delta settings: Integrating outcrop and ground-penetrating radar data. *Sediment. Geol.* **2017**, *362*, 83–100. [CrossRef]

96. Catuneanu, O.; Galloway, W.E.; Kendall, C.G.S.; Miall, A.D.; Posamentier, H.W.; Strasser, A.; Tucker, M. Sequence stratigraphy: Methodology and nomenclature. *Newsl. Stratigr.* **2011**, *44*, 173–245. [CrossRef]
97. Massari, F. Supercritical-flow structures (backset-bedded sets and sediment waves) on high-gradient clinoform systems influenced by shallow-marine hydrodynamics. *Sediment. Geol.* **2017**, *360*, 73–95. [CrossRef]
98. Leclair, S.F.; Arnott, R.W.C. Coarse-tail graded, structureless strata: Indicators of an internal hydraulic jump. In *Shelf Margin Deltas and Linked Down Slope Petroleum Systems: Global Significance and Future Exploration Potential*; Roberts, H.H., Rosen, N.C., Filion, R.H., Anderson, J.B., Eds.; SEPM: Houston, TX, USA, 2003; pp. 817–836.
99. Postma, G.; Kleverlaan, K.; Cartigny, M.J.B. Recognition of cyclic steps in sandy and gravelly turbidite sequences, and consequences for the Bouma facies model. *Sedimentology* **2014**, *61*, 2268–2290. [CrossRef]
100. Zhong, G.; Cartigny, M.J.B.; Kuang, Z.; Wang, L. Cyclic steps along the South Taiwan Shoal and West Penghu submarine canyons on the northeastern continental slope of the South China Sea. *Geol. Soc. Am. Bull.* **2015**, *127*, 804–824. [CrossRef]
101. Ventra, D.; Cartigny, M.J.B.; Bijkerk, J.F.; Acikalin, S. Supercritical-flow structures on a Late Carboniferous delta front: Sedimentological and paleoclimatic significance. *Geology* **2015**, *43*, 731–734. [CrossRef]
102. Lang, J.; Winsemann, J. Lateral and vertical facies relationships of bedforms deposited by aggrading supercritical flows: From cyclic steps to humpback dunes. *Sediment. Geol.* **2013**, *296*, 36–54. [CrossRef]
103. Fielding, C.R. Upper flow regime sheets, lenses and scour fills: Extending the range of architectural elements for fluvial sediment bodies. *Sediment. Geol.* **2006**, *190*, 227–240. [CrossRef]
104. Kostic, S.; Smith, I.B. Water on Mars: Do submarine cyclic steps exist on the Red Planet? *Prog. Earth Planet. Sci.* **2018**, *5*, 76. [CrossRef]
105. Parsons, J.D.; Bush, J.W.M.; Syvitski, J.P.M. Hyperpycnal plume formation from riverine outflows with small sediment concentrations. *Sedimentology* **2001**, *48*, 465–478. [CrossRef]
106. Mulder, T.; Syvitski, J.P.M.; Migeon, S.; Faugeres, J.C.; Savoye, B. Marine hyperpycnal flows: Initiation, behavior and related deposits. A review. *Mar. Pet. Geol.* **2003**, *20*, 861–882. [CrossRef]
107. Carter, L.; Gavey, R.; Talling, P.; Liu, J. Insights into submarine geohazards from breaks in subsea telecommunication cables. *Oceanography* **2014**, *27*, 58–67. [CrossRef]
108. Chiocci, F.L.; Casalbore, D. Submarine gullies on Italian upper slopes and their relationship with volcanic activity revisited 20 years after Bill Normark's pioneering work. *Geosphere* **2011**, *7*, 1284–1293. [CrossRef]
109. Gamberi, F.; Rovere, M.; Mercorella, A.; Leidi, E.; Dalla Valle, G. Geomorphology of the NE Sicily continental shelf controlled by tidal currents, canyon head incision and river-derived sediments. *Geomorphology* **2014**, *217*, 106–121. [CrossRef]
110. Martorelli, E.; Bosman, A.; Casalbore, D.; Falcini, F. Interaction of down-slope and along-slope processes off Capo Vaticano (southern Tyrrhenian Sea, Italy), with particular reference to contourite-related landslides. *Mar. Geol.* **2016**, *378*, 43–55. [CrossRef]
111. Mulder, T.; Syvitski, J.P.M. Turbidity currents generated at mouths of rivers during exceptional discharges to the world oceans. *J. Geol.* **1995**, *103*, 285–299. [CrossRef]
112. Plink-Björklund, P.; Steel, R.J. Initiation of turbidity currents: Outcrop evidence of hyperpycnal flow turbidites. *Sediment. Geol.* **2004**, *165*, 29–52. [CrossRef]
113. Ghienne, J.F.; Girad, F.; Moreau, J.; Rubino, J.L. Late ordovician climbing dune assemblages: A signature of outburst flood in proglacial outwash environments. *Sedimentology* **2010**, *57*, 1175–1198.
114. Mulder, T.; Alexander, J. The physical character of subaqueous sedimentary density flows and their deposits. *Sedimentology* **2001**, *48*, 269–299. [CrossRef]
115. Jopling, A.V. Hydraulic factors controlling the shape of lamina in laboratory deltas. *J. Sediment. Petrol.* **1965**, *35*, 777–791.
116. Marren, P.M. Magnitude and frequency in proglacial rivers: A geomorphological and sedimentological perspective. *Earth-Sci. Rev.* **2005**, *70*, 203–251. [CrossRef]

© 2019 by the authors. Licensee MDPI, Basel, Switzerland. This article is an open access article distributed under the terms and conditions of the Creative Commons Attribution (CC BY) license (http://creativecommons.org/licenses/by/4.0/).